N.A.Slavinskaya[1,2], A.Mirzayeva[1], R.Whitside[1], J.H. Starke[1], M. Abbasi[1], M.Auyelkhankyzy[1] and V.Chernov[3], A modelling study of acetylene oxidation and pyrolysis, Combust. Flame 210 (2019) 25-42.

https://doi.org/10.1016/j.combustflame.2019.08.024

A MODELING STUDY OF ACETYLENE OXIDATION AND PYROLYSIS

N. A. Slavinskaya[1,2], A. Mirzayeva[1], R. Whitside[1], J.H. Starke[1], M. Abbasi[1], M.Auyelkhankyzy[1]

[1]German Aerospace Center, Institute of Combustion Technology, Pfaffenwaldring 38-40, 70569 Stuttgart, Germany
[2] Gesellschaft für Anlagen- und Reaktorsicherheit (GRS) gGmbH, Forschungszentrum, Boltzmannstraße 14, 85748 Garching, Germany

and

V.Chernov[3]

[3]Ort Braude College, Department of Mechanical Engineering, Snunit 51, Karmiel, 2161002, Israel

This study initiates the gradual upgrade of the DLR reaction database. The upgrade plan has two main steps: an optimisation of the C_1-C_4 oxidation chemistry and a revision of the polyaromatic hydrocarbon (PAH) formation sub-mechanism based thereupon. The present paper reports the main principles applied to model improvements and results obtained for the acetylene (C_2H_2) oxidation sub-mechanisms. The principle acetylene oxidation reactions have been revised as well as the detailed chemistry of important intermediates, i.e. methylene, ethynyl, vinylperoxy radical and also diacetylene, vinylacetylene and higher diacetylenes, important for PAH formation. The uncertainty intervals of the studied reactions were statistically evaluated, providing general bounds for the performed modifications to reaction rate coefficients. The first stage of the presented update was performed through revision of the thermochemical data and model optimisation on ignition delay data and laminar flame speed data, since they exhibit lower uncertainty in comparison to species profile data. The final model optimization was obtained through simulations of concentration profiles measured in shock tubes and laminar flames for improvement of the reaction paths and rate coefficients related to acetylene pyrolysis and PAH precursor formation. Approximately 500 data points were analysed. The updated reaction mechanism predicts all simulated experimental data, also not included in the optimisation loop data prom plug flow and jet-stirred reactors, either with good or satisfactory agreement. It was found that the vinylperoxy radical formation and consumption dictate the reaction progress at low temperatures. The performed study clearly determined that acetylene combustion proceeds through the strongly coupled reaction paths of fuel oxidation and PAH precursor formation; the same species are involved in these parallel processes. Therefore, the self-consistent reaction model for acetylene combustion could be obtained only by an optimisation performed on the experimental dataset encompassing both processes.

Key words: acetylene, reaction mechanism, ignition, flame, aromatic molecules

1. Introduction

The progress of combustion chemistry necessitates revision of combustion models from time to time as new understanding and experimental and numerical tools emerge. This improves the reaction models of hydrocarbons for which new data were obtained and also for the connected sub-models, primarily for sub-models of pollution formation in combustion processes. Soot formation and growth is one of the most critical problems in combustion simulation due to the high level of the uncertainty of kinetic rate parameters, thermo- and transport data related to both the soot growth models and to the gas-phase formation of the soot precursors, i.e. polyaromatic hydrocarbons (PAH). Growth of the PAH molecules is initiated with reactions of small radicals (H, OH, CH_3, C_2H, C_2H_3, H_2CCCH, C_3H_4, C_4H, H_2CCCCH, C_4H_5, C_5H_5) and molecules (C_2H_2, C_4H_2, C_4H_4) involved also in the fuel oxidation channels. Therefore the uncertainty of the C_1-C_4 oxidation kinetics will propagate in the uncertainty of the PAH sub-mechanism.

The reaction model for PAH formation and growth developed by the authors [1-3] forms the base of the global reaction database of the DLR Institute of Combustion Technology extended to the n-hexadecane sub-model. The reaction database has a hierarchical structure and is developed through continuous improvement, validation and optimisation arising from new, more accurate understanding. The sub-mechanisms for the individual components can be used separately and in different combinations producing surrogate models for practical fuels. Each new block in the database is implemented without disturbing the mechanisms of the existing sub-models with minimal changes and extensions to the existing sub-mechanisms.

With the present paper we begin publication of results for the C_1-C_4 chemistry update, which was initiated with the acetylene (C_2H_2) oxidation sub-mechanisms. The principle objectives of the present study are: (a) to extend and improve the acetylene reaction sub-mechanisms of the model [2, 3]; and (b) to elucidate the evolution of the aromatics precursors in the studied systems and thereby to identify any further improvement potential. The model revision and extension have been performed on the basis of extensive literature analysis, uncertainty quantification of reaction rate coefficients and simulation of experimental data for ignition delay, laminar flame speed and concentration profiles measured in shock tubes, laminar flames and flow reactors. Special attention was paid to calculation of the kinetic parameter uncertainty for the most important reactions under the considered conditions. This update promotes future analysis and treatment of the DLR reaction database with an automated data-centric infrastructure Process Informatics Model (PrIMe) [4-6] towards to the more and more actual today “best estimate plus uncertainty (BEUP)” strategy.
Shortcomings in previous implementations (partially caused by mistakes in the used version of CHEMKIN code [7]) have been identified and corrected.

2. Agenda

The paper is organised as follows: the third section briefly reports the method applied for the evaluation of rate coefficient uncertainty; the fourth part presents the principle reaction rate uncertainty analysis further used for experimental target selection and for the C_2H_2 sub-model

extension and update performed first on the ignition delay and laminar flame speed data and subsequent on the concentration profile data. The final section presents results and discussion.

The present work is supported by the Supplement Materials-1,2,3,4,5 and by the online model presentation together with the entire experimental data set used for model validation, [8].

3. Uncertainty bounds of the reaction rate parameters

It is not currently feasible to use highly accurate first-principle calculations for each reaction encountered in the kinetic model: reliable experimental or theoretical thermochemical data is scarce; the uncertainties of the published reaction rate coefficients are often not available, even for "small hydrocarbon" chemistry. The reliance on experimental data for model validation creates an error propagation problem, further increasing overall uncertainty [4,5,9-12]. To keep the size of the feasible parameter region and to understand the intervals for the reaction rate coefficient modifications we performed the statistical analysis [13-15] (described in details in the Supplement-1) of the literature data.
The standard deviations of the Arrhenius expression parameters *A*, *n*, and E_a ,

$$k(T) = AT^n \exp(-E_a/T) \text{ , } (cm^3, s, mole, K) \quad (1)$$

calculated in the applied method, determine the margin, $\Delta k(T)$, of the rate-coefficient error. The uncertainty factor, $f(T)$, is used to determine the uncertainty level for $k(T)$:

$$f_u(T) = \log\left[\frac{k_{upper}(T)}{k_0(T)}\right]$$

$$f_l(T) = \log\left[\frac{k_0(T)}{k_{low}(T)}\right] \quad , \quad (2)$$

where k_0 is the nominal rate coefficient and k_{low} and k_{upper} are the lower and upper bounds, respectively.

The statistical treatment of the rate coefficients is complicated by the limited amount of available data, but if several datasets are present the simple analysis of uncertainty *k* based on the least-squares regression can be done (Supplement-1). The so obtained Arrhenius parameters give the mean, or nominal, values of the coefficients k_0, which on its own is not so interesting for the content of this paper, and also useful statistical information. Parameter errors, $s(x_\alpha)$, eq. (S1-6, Supplement-1), describe the confidence level of the rate coefficient parameters and can be further used for calculation of:

$$k_{low}(T) = (A - s(A))T^{(n-s(n))}\exp(-(E_a + s(E_a))/T), \quad (3)$$

$$k_{upper}(T) = (A + s(A))T^{(n+s(n))}\exp(-(E_a - s(E_a))/T) \quad (4)$$

and finally for an evaluation of the uncertainty factors, eq. (2).

4. C_2H_2 kinetical sub-model update: Model-1.

The C_2H_2 chemistry of [1-3] originated mostly from the Leeds mechanism [16], which was chosen in [1] for the PAH sub-model construction as a model with a minimal set of fitted data. The actual H_2/CO chemistry of the studied model is described in detail in [6] and the mechanism for the methane sub-model can be found in [8].

Several chemical-kinetic mechanisms for acetylene oxidation are available in the literature [17-28]. These studies highlight advancing knowledge in acetylene oxidation and pyrolysis, summarised in the general scheme shown in Fig.1 and adopted herein as a skeletal model for further development.

The available reaction rate parameters of acetylene oxidation chemistry are still fragmented and do not cover the full range of pressures and temperatures relevant to practical flames. Most of them were obtained either from a fitting procedure based on experimental observations in flames, shock tubes and flow reactors. A smaller sample of reaction rate coefficients is obtained from "direct" experiments, which, generally, are only nominally direct and from quantum-chemical calculations, which are generally dependent on theoretical assumptions [27, 29].

The model revision and modification began with a review and justification of the reaction rate coefficient sources with respect to the main reactions of the oxidation model, Figure 1.

The uncertainty bounds, f_u and f_l, were calculated from k_{low} and k_{upper}, evaluated using the numerical method of [13], Suplement-1. The approximations have been performed for all 3 parameters in the Arrhenius equation, eq. (1), if more than 3 literature sources for rate coefficients have been found and for 2 parameters (A and E_a) for a minimal dataset, *i.e.* 3 literature sources. If uncertainties of the literature data were available, they have been taken in the analysis and assigned to the weights, ω_j, of observations. If not, an error equal to 50% was initially assigned to the rate coefficient. Further in the treatment process, such values were reduced or increased accordingly.

4.1. Overview of the major initial reactions

The C_2H_2 interaction with O_2 is one of the dominant initiation steps (mostly at high temperature) proceeding through 3 possible channels (R1a-c) adopted in the present model:

$C_2H_2+O_2 \leftrightarrow CH_2O+CO$ (R1a)
$\leftrightarrow C_2H+HO_2$ (R1b)
$\leftrightarrow HCCO+OH$ (R1c)

Besides (R1a-c), four other paths, $C_2H_2+O_2 \leftrightarrow 2HCO$, $C_2H_2+O_2 \leftrightarrow H+CO+HCO$, $C_2H_2+O_2 \leftrightarrow CH_2+CO_2$ and $C_2H_2+O_2 \leftrightarrow CH_2OC+O$, are also described in the literature [26-29]. However, there is significant disagreement concerning product channels, key steps, reaction rates and branching ratios for these oxygen addition reaction channels [27]. The only channel

yielding HCCO+OH, (R1c), highly important for acetylene oxidation, was newly introduced in the model with the rate constant adopted from the mechanism of Miller and Melius [32].
The rate constant for the overall reaction $C_2H_2+O_2 \leftrightarrow$ *products* obtained by Laskin and Wang [30] with RRKM calculations has been assigned to channel (R1a), identified as favoured in [30]. The recommendation of Tsang and Hampson [33] was used for the (R1b) channel. The available information does not allow application of statistical methods to evaluate the uncertainty bounds for (R1a)-(R1c). The uncertainty factor of 1 proposed by Tsang and Hampson [33] for (R1b) has also been assigned to (R1a) and (R1c).
The other major initial stages of acetylene oxidation, (R2-R5) have been analysed and their reaction rate coefficients uncertainties have been evaluated, Table1, and Supplement-2.
As shown in Table 1 and Figures S2-1, the literature data is highly scattered for most studied reactions, leading to high uncertainty factors between 0.9 and 4.8, depending on temperature. Basically, $f_u(T)$ and $f_l(T)$ have the lowest values for the more widely investigated temperature intervals. The correlation coefficients for the Arrhenius parameters, eq. (1), calculated with eqs. (S10 andS11, Supplement-1) lay in the range 0.90-0.99 for all investigated reaction rate coefficients.

The reaction schemes of acetylene oxidation, shown in Figure 1, and most important mechanism extensions and modifications described above and in the Supplement-2, have been implemented in Model-1 as the first step of the DLR mechanism optimisation.

In comparison to oxygen addition, the reaction between acetylene and the hydroxide radical has been extensively investigated experimentally and theoretically. The analysis of numerous previous studies can be found in the work of Senosiain *et al.* [34]. The possible channels of the reaction between OH and C_2H_2 have been investigated in [21, 23, 30-38].

Liu *et al.* [35] experimentally investigated the overall reaction C_2H_2 + OH, without distinguishing the separate channels, at 1 atm in an argon buffer gas from 333 to 1273 K using the pulse radiolysis technique. Using a molecular-beam sampling technique, Vandooren and Van Tiggelen [36] evaluated rate coefficients for (R2b) and (R2c) from the study of the flame structure of a low-pressure lean and stoichiometric C_2H_2/O_2 burning mixture. Woods and Haynes [37] modified the rate coefficient for (R2b) evaluated in [32] through modelling of their experimental data for concentration profiles measured in premixed fuel-rich ethylene/air flames. They evaluated the error of this model as ± 30%.

Miller and Melius [38] calculated rate coefficients for (R2a)-(R2c) using BAC-MP4 and the addition reaction channel $C_2H_2+OH \leftrightarrow HOC_2H+H$ using potential-surface parameters and statistical-theoretical methods. The rate coefficient for (R2a) was also evaluated in the review of Tsang and Hampson [33] with an uncertainty factor 1. Lindstedt and Skevis [21] assigned the rate coefficient evaluated in [38] for the channel $C_2H_2+OH \leftrightarrow HOC_2H+H$ to the channel (R2b). Senosiain *et al.* [34] calculated rate coefficients for 5 different reaction channels of the C_2H_2+OH reaction using the RQCISD(T) method for a wide range of temperatures and pressures. These calculated values were adopted in the present model for (R2a)-(R2c) without significant loss of accuracy or general applicability of the reaction mechanism. The channels (R2b) and (R2c) are new additions to the model. The uncertainty bounds for the adopted

values have been estimated using data proposed in the studies [31-35, 38], see Figure 2. The graphics for all other investigated reaction rate coefficients can be found in Supplement 2, Figure S2-1. The intervals for obtained minimal and maximal values of $f_u(T)$ and $f_l(T)$ and the corresponding input parameters are summarised in Table 1.

Table 1. Uncertainty factors calculated from literature sources for major initial stages of acetylene oxidation. $k(T) = AT^n \exp(-E_a/T)$. Values adopted for Model-1 are printed in italics.

Reaction		Ref.	ΔT,K	k , cm^3,s, mole, K			Data Error, %	$f_u(T)$ and $f_l(T)$
				A	n	E_a		
(R2a)	C_2H_2+OH↔C_2H + H_2O	[38]	1000-2500	3.37E+07	2.0	7056	50	1.42-1.69
		[34]	500-2500	*2.60E+06*	*2.4*	*8586*	50	
		[33]	300-2500	1.45E+04	2.7	6060	50	
(R2b)	C_2H_2 + OH ↔CH_3 + CO	[38]	500-2500	4.83E-04	4.0	-1000	50	2.59-5.00
		[34]	500-2500	*1.23E+09*	*0.73*	*1298*	50	
		[36]	650-1100	5.50E+13	0.0	6905	50	
(R2c)	C_2H_2 + OH ↔CH_2CO+H	[21]	1180-2200	3.79E+06	1.7	503	50	2.46-4.10
		[22]	1000-2500	1.90E+07	1.7	505	50	
		[38]	500-2500	4.97E-17	4.5	-504	50	
		[36]	570-850	3.20E+11	0.0	101	50	
		[37]	1640-1950	1.10E+13	0.0	3614	50	
		[34]	500-2500	*7.53E+06*	*1.6*	*1060*	50	
(R3a)	C_2H_2 + O ↔ CH_2 + CO	[39]	300-2500	2.17E+06	2.1	790	50	1.54-1.81
		[40]	850-1950	7.23E+05	2.1	787	50	
		[41]	850-1950	6.12E+06	2.0	958	50	
		[42]	1500-2500	1.60E+14	0.0	4987	50	
		[43]	200-2500	*2.35E+08*	*1.4*	*1110*	50	
		[20]	1000-2000	2.08E+14	0.0	4990	50	
		[44]	300-2000	4.10E+08	1.5	843	50	
		[36]	300-1430	6.70E+13	0.0	2016	50	
		[45]	200-2000	7.40E+08	1.3	1236	50	
		[46]	1500-2570	1.20E+14	0.0	3300	50	
(R3b)	C_2H_2 + O ↔HCCO+H	[40]	850-1950	5.78E+06	2.1	787	50	1.28-1.70
		[41]	195-2500	1.43E+07	2.0	958	50	
		[42]	1500-2500	4.00E+14	0.0	5372	50	
		[43]	200-2500	*9.40E+08*	*1.4*	*1110*	50	
		[20]	1000-2000	5.20E+14	0.0	5393	50	
		[45]	200-2000	2.96E+09	1.3	1236	50	
		[21]	195-2500	6.30E+06	2.1	787	50	
(R3c)	C_2H_2 + O ↔C_2H + OH	[47]	500-2500	*4.60E+19*	*-1.4*	*14485*	50	2.52-2.74
		[32]	500-2500	3.16E+15	-0.6	7560	50	
		[48]	500-2500	3.00E+14	0.0	12600	50	
(R4)	C_2H+H(+M) ↔C_2H_2(+M), k_∞	[33]	200-2000	1.80E+13	0.0	0.0	50	2.00-2.5
		[47]	300-2500	*1.00E+17*	*-1.0*	*0.0*	50	
		[49]	200-2000	2.24E+13	0.32	0.0	50	
(R5)	C_2H_2+H(+M)↔C_2H_3(+M), k_∞	[16]	200-400	8.43E+12	0.0	1300	50	0.76-1.93
		[50]	300-2000	*1.71E+10*	*1.27*	*1354*	50	
		[44]	300-500	5.60E+12	0.0	1200	50	
		[43]	200-2000	5.54E+08	1.64	1055	50	
		[51]	200-3000	3.61E+10	1.09	1328	50	
		[52]	193-1600	4.40E+08	1.75	1222	50	

4.2. Model-1 validation and improvement of ignition delay time and laminar flame speed data

Model-1 is the first extension and modification of previous reaction mechanism [3], performed to describe the acetylene oxidation as it is shown in Figure 1, and was described in section 4.1 and in Supplement-2. Model-1 was tested against ignition delay time and laminar flame speed data [20, 26, 51-59], Table 2. The Chemkin package [7] and Chemical Work Bench software [62] have been used to simulate the experimental targets.

The first simulations revealed the progress in reproducing the ignition delay experimental data in comparison with simulations using the previous model [3]; the least-squares residual was reduced from 1.06E-03 to 7.91E-05, Figure S2-7. The major improvement in agreement between Model-1 and experiments is attributed to simulations of the shock-tube data of Fournet *et al.* [55]. The biggest disagreement (overprediction) with experimental data was obtained for ignition delay at lower, T < 1200K, temperatures [53, 55].
Both models, [3] and Model-1, exhibit high disagreement in both the values and overall trends (overprediction) of laminar flame speed for rich flames, at $\phi > 1.2$.

Experimental targets for Model-1 improvement.

Model improvement through modifications in the reaction rate coefficients has been completed using select experimental targets, based on a comparison of the normalised integrated sensitivity coefficients, S_{ij}, of ignition delay times and laminar flame speeds, the reaction rate uncertainties (collected in Table 1) and experimental errors, ε.
The sensitivity coefficients of all experimental data used for model validation were calculated as a response of the model output δ_i^{out} to the perturbation in pre-exponentials, δ_j^{par}, in the Arrhenius reaction rate expression, eq. (1), $S_{ij} = \delta_i^{out} / \delta_j^{par}$. The perturbations in the pre-exponentials were chosen to equal the maximum uncertainty of the studied rate coefficients, Table 1.

Table 2. Experimental ignition delay time and laminar flame speed data used for model improvement.

Authors	Ignition delay	Laminar flame speed	
	Shock tube	Counterflow flame	Spherical flame
Rickard *et al.* [53]	$C_2H_2/O_2/Ar$ T_5=1098-2319 K, p_5=1 bar, φ=0.5-0.53		
Eiteneer and Frenklach [26]	$C_2H_2/O_2/Ar$ T_5=1151-2132 K, p_5=1-1.9 bar, φ=0.0625-1.4		
Hidaka *et al.* [20]	$C_2H_2/O_2/Ar$ T_5=1055-1629 K, p_5=1.1-2.1 bar, φ=0.49-2.0		
Fournet *et al.* [55]	$C_2H_2/O_2/Ar$ T_5=1011-1381 K, p_5=8.5-10.0 bar, φ=0.3125-0.625		
Egolfopoulous *et al.* [56]		C_2H_2/air, T_0= 298K p=1 bar, φ=0.6-1.8	

Authors	Ignition delay	Laminar flame speed	
	Shock tube	Counterflow flame	Spherical flame
Park *et al.* [58]		C_2H_2/ O_2/ N_2 T_0=298K p=1 bar, φ=0.7-1.7	
Jomaas *et al.* [57]			C_2H_2/air, T_0=298K p=1,2 bar, φ=0.7-2.0
Ravi *et al.*, [59]			C_2H_2/air, T_0=298K p_0=1-2 bar, φ=0.6-2.0
Shen *at al.*, [60]			C_2H_2/air, T_0=298K p=1bar, φ=0.6-2.0 p=1-20 bar, φ=0.8; 1.6
Rokni *et al.*, [61]			C_2H_2/air, T_0=298K p=1, φ=0.6-2.0

The measured data have been used for rate coefficient improvement if δ_i^{out}, obtained through the parameter perturbation (δ_j^{par}), was higher than the experimental error, i.e. $\varepsilon \leq \delta_i^{out}$. By dividing both sides of this inequality with δ_j^{par}, the criterion for applicability of an experimental target, E_{ap}, for reaction rate improvement was obtained:

$$S_{ij} \geq E_{ap},\ E_{ap} = \varepsilon/\delta_j^{par}. \quad (5)$$

This condition alone is insufficient for selection of an experimental target suited to model improvement; S_{ij} must have a relatively high value compared to other coefficients.

An example of a comparison between S_{ij} and E_{ap} obtained for reaction (R2b) is demonstrated in Figure 2. The other comparisons can be found in Fig. S2-2. It can be seen that reaction (R2b), with the highest rate coefficient uncertainty, has a large number of experimental targets applicable for reaction rate improvement, Fig. 2. But, the investigated processes have very low sensitivity to (R2b), such that only the select few experimental datasets having the largest S_{ij} can be used for optimisation of k_{2b}.

The experimental errors, ε, for shock tube measurements were evaluated from the empirical rules described in [6].

In this way, applying criterion eq. (5), the ignition delay targets appropriated for the Model-1 improvement were reduced from 259 to 125 and combined with three laminar flame speed datasets measured for conditions p = 1 atm, T_0 = 298 K and ϕ = 0.6, 1.4 and 2.0.

Optimisation of rate coefficients

The reaction rate coefficients to be optimised were identified from the sensitivity and rate-of-production analysis performed for ignition delay times and laminar flame speed data calculated during the modelling of experimental data under different operating conditions with varied agreement between measured data and simulations. The aim of model analysis was to explain and improve a) the faster predictions of ignition delay times at T > 1700K; b) the slower one at T < 1200K; and c) the overprediction of laminar flame speed at ϕ > 1.2. Reactions with both high sensitivities and high accuracy of rate coefficients, $H+O_2 \leftrightarrow O+OH$,

HCO+M↔H+CO +M and CO+OH↔CO_2+H, HCO+H↔H_2+CO, were maintained at the rate values adopted in the model.

Figure S2-3, Supplement-2, provides analyses performed for ignition delay data. Sensitivity coefficients of atmospheric laminar flame speed at $\phi = 0.6$, 1.4 and 2.0 are shown in Figure 3. It can be observed in Figures S2-3, that for all simulated targets the same reaction pool influences the ignition delay time in the same manner, either promoting or suppressing the ignition, and is also important for laminar flame speed modelling, Fig.3. As expected, reactions (R3a,b,c) and (R4a,b,c) have the greatest impact on the oxidation process.

High-temperature ignition

High-temperature ignition, T_5>1200K, was mainly sensitive, Fig. S2-3, to the newly adopted initiation channel:

$C_2H_2+O_2 \leftrightarrow$ HCCO+OH. (R1c)

It was concluded that the value used in the mechanism Miller and Melius [32] for this channel should be considered as the overall reaction rate for all possible channels (R1a,b,c). The pre-exponential factor of k_{1c} from [32] was decreased through the model optimisation by factor of 10. Figure S2-8 demonstrates the final brunching ratios for (R1a,b,c). That resulted to the better describing the high-temperature ignition delay data. The following reactions of oxygen with ketenyl produced in (R1c) and the subsequently formed formyl radicals were consequently revised:

HCCO+O_2=CO_2+CO+H (R6a)
HCCO+O_2=HCO+CO+O (R6b)
HCCO+O_2=2CO+OH (R6c)
HCO+O_2=OH+CO_2 (R7a)
HCO+O_2=HO_2+CO (R7b)

The rate coefficients for (R6a,b,c) predicted with trajectory and master equation simulations by Klippenstein *et al.* [63] were finally adopted. For all temperatures considered in [63] (300–2500 K) the dominant products were CO_2+CO+H, independent of pressure up to 100 atm. Calculations [63] also predict minor branching to OCHCO +O and 2CO+OH.
The branching ratio for reactions of the formyl radical with oxygen (R7a,b), $k_{7a}/\ (k_{7b} + k_{7a})$, was finally modified in accordance with comments provided in [43] and assumed as 0.9. Finally, the possible influence of H_2CC and HOCO radicals on the high-temperature ignition modelling has been carried out. Performed simulations and kinetic analysis showed that these reactions did not have any impact on the studied processes, such that these species were removed in subsequent improvements to the model.

Low-temperature ignition

The performed analysis shown, that the low-temperature oxidation is inhibited with C_2H_3 formation/decomposition in (R5), Fig. S2-3. It was figured out, that an acceleration of ignition at low-temperatures, experimental data mostly from [54,55] for T < 1200K, could be achieved

through acceleration of the subsequent reactions of C_2H_3, which promote the acetylene oxidation chain and compete with vinyl decomposition or its accumulation. At that a boost of the reaction rate coefficient

$C_2H_3+O_2 \leftrightarrow CH_2O+HCO$ (R8)

conflicts with its promoting impact on the laminar flame speed. On this way, the reaction mechanism was extended with channels of vinyl oxidation, detailed investigated in the study of Goldsmith et al. [29]:

$C_2H_3+O_2=CH_2CO+OH$ (R9)
$C_2H_3+O_2=CH_2O+H+CO$ (R10)
$C_2H_3+O_2=CH_3O+CO$ (R11)
$C_2H_3+O_2=CO_2+CH_3$ (R12)
Also, for two channels
$C_2H_3+O_2=CH_2HCO+O$ (R13)
$C_2H_3+O_2=C_2H_2+HO_2$ (R14)

k_{13} and k_{14} were newly adapted from study [29]. The $C_2H_3 + O_2$ reactions play a key role for the acetylene oxidation, but, due to lack of rate coefficient data we could perform the uncertainty analysis only for k_8, Fig.S2-4. The rate value calculated by Mebel *et al.* [64] multiplied with 2 was prescribed to k_8 finally.

Tangible progress in the low temperature ignition simulations was obtained after introduction of the formation/consumption of the vinylperoxy radical [27, 29, 64-66]. The vinylperoxy is produced in barrierless vinyl + O_2 reaction and further, with temperature increase, is decomposed in the chain branching reactions:

$C_2H_3+O_2=CH_2CHOO$ (R15)
$CH_2CHOO =CH_2CO+OH$ (R16)
$CH_2CHOO =CH_2O+H+CO$ (R17)
$CH_2CHOO =CO+CH_3O$ (R18)
$CH_2CHOO =CO_2+CH_3$ (R19)
$CH_2CHOO =CH_2HCO+O$ (R20)
$CH_2CHOO=CH_2O+HCO$ (R21)

The k_{15} was studied by Da Silva *et al.* [66] using variational transition state theory, with O3LYP/6-31G(d) potentials scaled by G3B3 reaction enthalpies, and illustrated that the vinyl + O_2 reaction occurs via two discrete channels: cis- and trans-vinylperoxy. The most comprehensive study was arguably performed by Goldsmith *et al.* [29]. The temperature- and pressure-dependent rate coefficients for reactions related to CH_2CHOO were calculated based on state-of-the-art calculations of the $C_2H_3O_2$ potential energy surface and was finally adopted in the model. The comparison of the rate coefficients calculated in [66] and [29] is shown in Fig. S2-5 of Supplement-2. Despite of the big deference in the rate coefficients calculated in [29] and [66] these values did not noticeably impacted the results of simulations. But for the cool flames we obtained the better convergence at calculations if the k_{15} from Da Silva *et al.* [66] was used. This value finally multiplied with 2 was adopted in the model.

The accuracy of laminar flame speed simulations was further improved by increasing the branching ratio $k_{3b}/\ (k_{3b} + k_{3a})$ to 0.9.
The described modifications, performed to improve simulations of ignition delay times and laminar flame speed data, resulted in Model-2.
Sensitivity analysis of the flame speed at higher equivalence ratios (sooting flames), Fig. 3, revealed the moderate importance of reactions of the important PAH precursors:

C_4H_2+OH ↔ C_3H_2+HCO (R22)
i-C_4H_5↔C_2H_3+C_2H_2 (R23)
C_4H_4+O↔C_3H_4+CO (R24)
C_2H_2+C_2H↔ C_4H_2+H (R25a)
H_2CCCH+OH↔HCO+C_2H_3 (R26)
C_2H_2+CH↔H_2CCCH. (R27)

Due to their relatively low impact on the laminar flame speed data and general insignificance for ignition delay time, these experimental targets, eq. (5), could not be used for further insight into reactions (R22)-(R27). The revision and validation of the chemistry of H_2CCCH, C_4H_2, C_4H_4, i-C_4H_5 have been performed on simulations of concentration profiles measured in laminar flames, shock tubes and plug flow reactors (PFR). This enabled the next step of Model-2 improvement without sacrificing the quality of the simulations.

4.3. Model-2 validation and improvement of concentration profile data from shock tube, laminar flame and plug flow reactor measurements

The revision and analysis of the production/consumption of H_2CCCH, C_4H_2, C_4H_4 and i-C_4H_5 was carried out on the species profiles measured in shock tubes [67-70], laminar flames [19, 71-73] and flow reactors [31, 74, 75], Table S3-1, Supplement-3. A summary of the species measured in those experiments is provided in Table 3, showing that the main investigated species are products of acetylene oxidation and pyrolysis. Nonetheless, an optimisation for the target species which were measured in 3 or more works was performed. It should be noted, that some datasets have varying quality and occasionally noticeable ambiguity in the operating conditions and therefore were used only for the model validation, but not for the optimisation.

Table 3. Species measured in experimental studies used for model improvement.

	Shock Tube				Laminar Flame				PFR		
	[67]	[68]	[69]	[70]	[71]	[72]	[19]	[73]	[31]	[74]	[75]
C_2H_2	x	x	x	x	x	x	x		x	x	x
O_2					x	x	x				
H					x	x					
OH					x	x	x				
H_2						x				x	
H_2O					x	x	x				
CO_2					x	x	x		x		
CO					x	x	x		x		

	Shock Tube				Laminar Flame				PFR		
	[67]	[68]	[69]	[70]	[71]	[72]	[19]	[73]	[31]	[74]	[75]
CH							x				
CH_3					x						
CH_4										x	x
HCO					x						
C_2H						x					
C_2H_3					x						
C_2H_4									x	x	x
C_3H_2					x						
H_2CCCH					x			x			
H_2CCCCH						x		x			
C_3H_4					x						
C_4H_2	x	x	x	x	x	x	x				
C_4H_4	x					x				x	
C_4H_5						x		x			
C_5H_5								x			
C_5H_6								x			
A1	x					x		x		x	x
$A1C_2H$	x										
C_6H_2	x	x	x	x							
C_8H_2				x							
A2											x
A2R5											x
A3										x	x
A4										x	x
Chrysene										x	
BAPYR										x	x

Alzueta *et al.* [31] reported an uncertainty of approximately 80% for their measured C_2H_4 concentration. As we did not find other error analyses, we assigned this uncertainty to all of the experimental concentration profiles from PFR studies [31, 74, 75], which were measured with the similar methodology and gas chromatography. For the concentration profiles from the shock tube data [67-70] uncertainty factor of 2 has been assumed. For the laminar flame data [19, 71-73] an error of about 30% was assumed based on the empirical rules described in [6].

Through review of the acetylene oxidation reaction models and experimental data one can conclude that a large part of acetylene pyrolysis reactions and their rates follow from early shock-tube studies [20, 67-69]. Simplified reaction models have been developed/validated/fitted to these experimental results, leading to inaccuracies in future models based thereupon. Preliminary revision of the studied model showed that reaction $2C_2H_2 \leftrightarrow C_4H_2 + H_2$ can be eliminated from the model, because it is a sum of two reactions (R26) and:

$2C_2H_2 \leftrightarrow H_2CCCCH + H$ (R28)

Also, reaction $C_4H_2+H_2 \leftrightarrow C_4H_4$, which appears in some literature models, is a sum of $2C_2H_2 \leftrightarrow C_4H_2+H_2$ and

$C_4H_4 \leftrightarrow 2C_2H_2$. (R29)

The preliminary simulations of data from Table 3 with Model-2 demonstrated good agreement with experimental data for the main reaction products and the H_2CCCH radical, overpredicts C_4H_2 and i-C_4H_5 concentration profiles and underpredicts production of H_2CCCCH, C_6H_2 and C_8H_2. As the species C_2H_2, C_4H_2 and C_6H_2 are the most widely investigated, Table 3, their concentration profiles were the main targets for further improvement.

The reaction rate analyses showed that C_4H_2 and C_6H_2 production is strongly dependent on the competing C_2H radical consumption in reactions:

$C_2H_2+ C_2H \leftrightarrow C_4H_2+H$ (R25a)
$C_2H_2+ C_2H \leftrightarrow H_2CCCCH$ (R25b)
$C_4H_2+ C_2H \leftrightarrow H+C_6H_2$ (R30)

The underprediction of H_2CCCCH, C_6H_2 and C_8H_2 by Model-2 arose from a deficit of the C_2H radical, mostly consumed for C_4H_2 production in step (R25a). The main reaction steps giving C_2H are (R2a), (R4) and:

$C_2H_2+H \leftrightarrow H_2+ C_2H$ (R31)

An increase in the production rates of H_2CCCCH and C_6H_2 and a simultaneous decrease of C_4H_2 production was achieved through balancing of the C_2H and C_4H_2 production/consumption in last cited reactions and in reactions favour the formation of C_4H_2:

$H_2CCCCH+H \leftrightarrow C_4H_2+H_2$ (R32)
$C_4H_2+H(+M) \leftrightarrow H_2CCCCH(+M)$ (R33)

The pressure-dependent reaction (R33) investigated by Klippenstein and Miller [76] was adopted in the model instead of monomolecular H_2CCCCH decomposition after revising the analysed reaction sequence. Also the rate coefficient value recommended in Slagle *et al.* [77] is now used instead of that from Miller and Melius [32] for reaction

$H_2CCCCH+O_2=CH_2CO+HCCO$. (R34)

Three new reactions involving diacetylene decomposition and H abstraction:

$C_4H_2 \leftrightarrow 2C_2H$ (R35)
$C_4H_2+M \leftrightarrow C_4H+H+M$ (R36)
$C_4H_2+OH \leftrightarrow C_4H+H_2O$, (R37)

were included in the model with k_{35} from [68] and k_{36} from [78]. The value of k_{37} was estimated by analogy to the reaction $C_4H_2+OH \leftrightarrow C_3H_2+HCO$ studied by Warnatz [44].

The important "bridge reaction" between small chemistry and the formation of first aromatic ring (R23) was revised. The earlier used experimental data for unimolecular decomposition from Dean [79] was analysed and finally changed to the second order reaction (R38) with k_{24} following from Weissman and Benson [80]:

$i\text{-}C_4H_5 + M \leftrightarrow C_2H_3 + C_2H_2 + M$ (R'23)

Reactions of polyynes production $C_4H_2+C_4H \leftrightarrow H+C_8H_2$ [69], $C_4H_2+C_4H_2 \leftrightarrow C_6H_2+C_2H_2$ [81], $C_4H_2+C_4H_2 \leftrightarrow C_8H_2+H_2$ [81] and $C_2H+C_4H \leftrightarrow C_6H_2$ have been tested through simulations. The simulations revealed that these reactions reach equilibrium, shifted to the right side, relatively quickly, only slightly influencing polyyne decomposition at high temperatures and generally not impacting polyyne production. These reactions were not included in the final model. Similarly, the H_2CC radical did not result in any impact on the modelling results.
For the key reactions (R25a,b), R(28), (R30) and (R32), the uncertainty intervals were evaluated with eqs. (3,4), Table S3-2 and Figure S5. Finally, an desired increase of H_2CCCCH and C_6H_2 concentrations and simultaneous decrease of the concentration of C_4H_2 has been achieved with modifications of k_{25a}, k_{25b}, k_{28} , k_{29}, and k_{31} described in the Table S3-2, Supplement-3.
Unfortunately, the extensive study of Zador et al. [82] came into sight after the final analysis and model validation was done. As studied acetylene mechanism is the part of DLR reaction base, every sub-models included in reaction base are tested after modifications performed for the C1-C2 chemistry. That is time-consuming process, because only modifications leading to the improvement in the sub-models involved are finally adopted. However, as it can be seen from Fig. S3-6, the calculations of the rate coefficients for the association of two acetylene molecules and related reactions performed by Zador et al. [82] applying the rigorous ab initio transition-state theory master equation methods lie in the calculated in this study uncertainty intervals. We would like to note that the increase of k_{28} during model optimisation on "the event-related phenomena" is in accordance with the results obtained in [82], what supports our strategy. The finally evaluated rate coefficient value for (R28) is slightly higher than the k_∞ value from [82], what follows from the lumping of the CCH_2 radical. The full implementation of the results gained in the [82] will be performed during the model update devoted to the PAH sub-mechanism improvement.

The performed modifications were implemented in the final Model, which is discussed in the next sections.
The reaction rate modifications we obtained through the simulations can be found in the Table S3-3, Supplement-3.

5. Results and discussion

5.1.Small PAH precursors

The obtained progress in simulations of concentration profiles of C_4H_2, H_2CCCCH, C_6H_2 and $i\text{-}C_4H_5$ measured in shock tubes [67-70] and laminar flames [71-73] is shown in Figures 4-6 and Figures S4-1-7 of Supplement-4. At the same time, the Model-2 and final Model match

concentrations of C_2H_2 and main reaction products equally well, showing that the modifications, performed for the PAH precursors, did not disturb the earlier accomplished quality of the fuel decomposition and oxidation process. Any other modifications led to loss of this performance.

The described above modifications led to a remarkable decrease of the simulated C_4H_2 concentrations at relatively low temperatures (< 2150K), if shock tube pyrolysis experiments was modeled, Table S2, Figures 4 and S4-1-4. At intermediate (2150-2350K) and high temperatures (> 2400K) the attained concentration decrease was slower or negligible. Consequently, the most effective improvement in the C_6H_2 shock tube data simulations was obtained at the lower and intermediate temperatures, Figures 4 and S4-1 and S4-2. At the high temperatures, Figure 4b, the increase in C_6H_2 production was observed only in the earlier stage of the processes before the equilibrium of reaction (R30) shifts to the left side. It was supposed that at the higher temperatures, another reaction mechanism, not connected to C_4H_2 production, affects the polyene formation. This could be the dehydrogenation of the linear C_6H_6, which is currently not included in the model. This extension will be performed as part of the improvement to the PAH formation sub-mechanism, after final upgrade of the C_3-C_4 sub-models.

Modelling of the target species measured in laminar flames, Table S3-1, also shows improvements through the model optimisation, Figures 5, S4-5-7. For simulations of the Bastin *et al.* [72] flat flame, their uncertainties of the flame temperature were incorporated. The presented results were obtained for the "averaged" temperature profile, shown in Fig. S4-6a as a dash-dot line. Due to inconsistencies in the measured data, the final simulations resulted in a compromise between the slight overprediction of the C_4H_2 data from the flat-flame burners of Bastin *et al.* [72] (Fig.5c) and Miller *et al.* [19] **(**Fig.5f), and the light underprediction of the C_4H_2 data measured by Westmoreland *et al.* [71], Fig.5b. Competing trends can also be seen in the concentrations of the H_2CCCCH measured by Bastin *et al.* [72], Fig.5d, and by Lamprecht *et al.* [73]**,** Fig.6b: the model overpredicts the data from [72] and underpredicts that of [73]. At the same time, model optimisation performed on these flames resulted in improvements to the i-C_4H_5 concentration modelling, Fig.5d and Fig.6f.

Generally, a good or satisfactory agreement, not exceeding a factor of 2, is achieved for all simulated species, major products, small radicals and PAH precursors. The performed optimisation of the C_4H_2, H_2CCCCH, C_6H_2 and i-C_4H_5 concentration profiles has resulted in progress to the reproduction of the propargyl radical, cyclopentadiene (C_5H_6) and the C_5H_5 radical, Fig.6a,c,d. The unregular behaviour of the i-C_4H_5 concentration profiles, Fig.5d, 6f, is related to the uncertainty of rate coefficient [R23'] at temperature < 1000K. Benzene prediction was consequently improved, Fig.6e.

For the lower temperatures (< 1200 K), the main reactions of the first single-ring molecule formation are

$C_7H_7 \leftrightarrow C_5H_5+C_2H_2$ (R38)

$H_2CCCCH+C_2H_2 \leftrightarrow$ A1- (R39)

i-$C_4H_5+C_2H_2 \leftrightarrow$ A1+H (R40)

With temperature increase (>1200K), the equilibrium of reactions i-C_4H_5 $+M \leftrightarrow C_2H_3+C_2H_2+M$ and reaction of cyclopentadienyl formation

$C_5H_5 \leftrightarrow H_2CCCH + C_2H_2$ (R41)

is shifted to the right and the H_2CCCH recombination determines the production of the first aromatic rings by over the entire reaction time. The role of (R39) in the phenyl production goes down with reduction of the acetylene concentration in the system.

The propargyl radical is formed at these conditions solely in two steps (R27) and:

$C_2H_2 + CH_2(S) \leftrightarrow H_2CCCH + H$ (R42)

We analysed sensitivity coefficients of the H_2CCCH, H_2CCCCH, i-C_4H_5 and C_5H_5 for different temperatures and for 60% and 80% of fuel consumptions.

For the lower temperatures (< 1200 K), reactions of C_2H_3, CH_2CHOO and CH_2HCO are mostly important for the H_2CCCH production, especially on the beginning of the fuel oxidation, Fig.7a-d. For the higher initial temperature, these reactions are further not important, Fig.7e,f: the production/consumption of propargyl radical is defined by reactions of CH, CH_2, C_3H_4 and benzene.

The change of dominant reactions with temperature for cyclopentadienyl is shown on the Fig.8. For the lower temperatures (< 1200 K), production of C_5H_5 is also mostly sensitive to reactions of C_2H_3, CH_2CHOO and CH_2HCO on the earlier stage of overall reaction, and to reactions of phenoxy radical if 80% of acetylene is destructed. The phenoxy production starts with (R39) in competing with (R38) and (R40). The consumption of C_5H_5 is dominated by benzyl production in (R38) at lower temperature, Fig.8a-d. For temperatures >1200 K, thorough the shift in the (R41), C_5H_5 is utilized mostly for the propargyl production and is mostly sensitive to its reactions, Fig.8e,f. The similar conclusions can be done for the sensitivity analyses performed for H_2CCCCH and i-C_4H_5.

The results of sensitivity analysis, Fig.7 and 8 highlight the tight coupling between components responsible for the oxidation and aromatics.

5.2.Acetylene oxidation

The described above model optimisation performed on the concentration profiles led to further progress in ignition delay time simulations (the least-squares residual was reduced from 7.91E-05 to 1.30E-05), Fig. 9 and Supplement-5; and in laminar flame speed modelling, Fig.10.

5.3.Blind Modeling

In order to test the model capabilities to reflect the physicochemical properties of the acetylene combustion, we performed the 'blind' modelling, i.e. simulations of experimental data obtained under different operating conditions and not used for the model optimization.

Laminar flame speed data at p=2 atm from Jomaas et al. and Ravi et al. [57, 59], and high-pressure data from Shen et al. [60], are shown in the Fig.11a,b. Flame data for lean mixtures, Fig.11b, is slightly overpredicted for p = 5-15 atm, and is in good agreement with simulations for p < 5 atm and p > 17 atm. For rich mixtures, the entire investigated pressure interval is well reproduced, excluding pressures below 5 atm, which conflicts with the data of Jomaas *et al.* [57] and Ravi *et al.* [59], Fig.10 and Fig.11a.

The concentration profiles from Alzueta et al. [31], Fig.12 and S4-11 have an excellent agreement with simulations.

Since we do not improve the PAH sub-model in this study, we used the data measured in plug flow and jet-stirred reactors by Norinaga et al. [74], Sanchez et al. [75] and Wang et al. [28] only for blind simulations, Figs. S4-8-10.

Unfortunately, it is difficult to understand the real uncertainty of the published data obtained in tubular flow or jet stirred reactors. The authors prefer to report a partial information concerning experimental errors. An essential problem of the tubular flow and stirred reactors is the assumption that the processes in these reactors are homogeneous, spatially uniform and stationary, i.e. "limited" only by chemical reaction kinetics and can be modelled with numerical models of PFR (1D) and PSR (0D). Therefore, experimental uncertainties of the tubular flow or jet stirred reactors characterize more the departure of the measured concentrations from an ideal case. Based on the investigations [7, 83-86] we evaluated systematic error conditioned by the reactor design, equipment and assumptions used in numerical models [7] as 25%-35%. For a random error we assumed evaluations performed by Norinaga et al. 2008 [74] for the *ex-situ* gas chromatography measurements: ±9% for gaseous, ±28% for major condensing products, and ±32% for minor condensing products (mainly PAHs). On this way, we can obtain, that departure of the measured concentrations from an ideal case lies in interval 30%-70%. For concentration uncertainties, we assumed 30% for small molecules, 50% for the one ring aromatic molecules, and 70% for the larger PAH, Fig. S4-8-10. Some details can be further found in the Supplement-4.
Many compounds were identified and analysed in these studies, ranging from small radicals to PAHs up to coronene ($C_{24}H_{12}$). All "small" molecules measured in these studies are reproduced within uncertainty intervals. For 6 species: CH_3CHO from Wang et al. [28], and C_8H_{12} from Norinaga et al. [74], $C_6H_5CH_3$ from Wang et al. [28], $C_{12}H_8$ from Sanchez et al. [75], A2 from Sanchez et al. [75], and $C_{16}H_{10}$ from Norinaga et al. [74] the largest disagreements were obtained reaching factor of 4-10, Figures S4-8-10. Benzene is undepredicted for both, Norinaga et al. [74] and Sanchez et al. [75], experiments with a factor of 2-2.5 and overpredicred for Wang et al. [28] with a factor of 3.
Nevertheless, simulations of these datasets demonstrate satisfying agreement, indicating that the performed model improvements resulted in an adequate self-consistent reaction mechanism with a high degree of reliability.
In the future work, devoted to the PAH sub-model, these data will be analysed more detailed.

5.4.Reaction-pass analysis

Figures 13 and 14 and S4-12 highlight the main chemical pathways of acetylene oxidation for the two temperatures 1150 K and 1650 K. The reaction flow diagrams were analysed for three time points: 10%, 30% and 80% of fuel consumption.
As shown in Fig.13a, C_2H_3 and HCCO are confirmed to be the dominant species in C_2H_2 oxidation below temperatures of 1300 K. Acetylene is primarily consumed by three reactions:

$C_2H_2+OH \leftrightarrow CH_2CO+H$ (R2c)
$C_2H_2+O \leftrightarrow HCCO+H$ (R3b)
$C_2H_2+H(+M) \leftrightarrow C_2H_3(+M)$ (R5)

The subsequent reactions of the ketenyl radical, HCCO, mostly yield CO and CO_2 (in agreement with the conclusions of Klippenstein *et al.* [63]), whereas oxygen addition to C_2H_3 in (R15) leads to vinylperoxy, CH_2CHOO and further to CH_2HCO and CH_2CO. The successive reactions (R16-R21), implemented in the current study, primarily dictate the subsequent reaction pathways, in turn accelerating C_2H_3 consumption and formation of active CH_2O, HCO and final products.

During the oxidation process, as temperature increases (Fig. 12b), HCCO becomes the dominant species and now primarily determines kinetics through reactions (R6a), (R6c) and $H+HCCO \leftrightarrow CH_2+CO$.

For initial temperatures above 1300 K, Fig.14, reaction (R3b) remains the main channel of fuel decomposition. The formation of the CH, CH_2 and C_2H radicals become important and strongly influence acetylene consumption:

$C_2H_2+OH \leftrightarrow C_2H+H_2O$ (R2a)
$C_2H_2+OH \leftrightarrow CH_2CO+H$ (R2c)
$C_2H_2+O \leftrightarrow CH_2+CO$ (R3a)
$C_2H+H(+M) \leftrightarrow C_2H_2(+M)$ (R4)
$C_2H_2+CH \leftrightarrow C_2H+CH_2$ (R27b)
$C_2H_2+H \leftrightarrow H_2+C_2H$ (R31)
$O_2+CH \leftrightarrow CO+OH$ (R43)
$O_2+CH \leftrightarrow CO_2+H$ (R44)
$O_2+C_2H \leftrightarrow CO_2+CH$ (R45)

The reactions of vinylperoxy do not significantly influence oxidation at initial temperatures above 1300 K.

We collected all reaction analysed in the paper with their used/optimised rate coefficients and uncertainty intervals (calculated, following from literature or evaluated after analogy) in the Table S3-3.

Conclusions

The update of the acetylene (C_2H_2) combustion sub-mechanism of the DLR reaction database has been successfully performed. The major initial stages of acetylene oxidation and pyrolysis, some associated secondary reactions and reactions related to PAH precursor formation have been revised. The obtained model was successfully validated against: (a) shock tube experimental data for ignition delay times in the range of pressure p_5 = 1-10 bar, temperature T_5 = 1000 – 2300 K, equivalence ratio φ = 0.0625-2; (b) laminar flame speed data for p = 1-20 bar, T_0 = 298 K, φ = 0.6-2; and (c) concentration profiles from laminar flames at

p = 0.026-0.050 bar, T_0 = 298-800 K, φ =1.67-2.5, shock tube pyrolysis measurements at p_5 = 0.3-8.0 bar, T_5 = 1100-2600 K, and plug flow reactors at p = 0.08-1.00 bar, T_0 = 700-1500 K, φ =0.06-1.43.

Approximately 500 experimental targets were analysed for model improvements. They were selected by the criterion of the experimental target applicability for model improvement, E_{ap}. The modifications of rate constants were performed within the uncertainty intervals estimated with statistical methods applied to the thermochemical data obtained from the literature. The deficit of experimental data useful for the kinetic model optimisation has been noted.

The model improvement was performed in a stepwise manner: the first stage of the update was performed through revision of the thermochemical data and model optimisation on ignition delay data and laminar flame speed data, since they exhibit lower uncertainty in comparison to species profile data. The final model tuning was obtained through simulations of concentration profiles measured in shock tubes, plug flow reactors and laminar flames.

The results of the first phase of optimisation positively influenced predictions of the target species under study during the second step. The model modifications performed on the small PAH precursor simulations conversely led to improvements of the ignition delay time predictions. This, coupled with good agreement of modelling results with the blind experimental data not involved in the optimisation process allows the conclusion that the developed model is self-consistent.

It was found that successive reactions of the vinylperoxy radical formation and consumption dictate the reaction progress at low temperatures. The implementation of these reaction routes into the current model led to significant progress in simulations of ignition delay times at temperatures below 1300 K. For initial temperatures above 1300 K, HCCO, mostly produced in C_2H_2+O↔HCCO+H, becomes the dominant species and primarily determines the high-temperature kinetics through the reactions HCCO+O_2=CO_2+CO+H, HCCO+O_2=2CO+OH and H+HCCO↔CH_2+CO.

The possible influence of H_2CC and HOCO radicals and their related reactions on the ignition process has been investigated. Performed simulations and kinetic analysis showed that these reactions did not change any simulation results and did not have any impact on the studied processes.

Revision and analysis of the production/consumption of H_2CCCH, C_4H_2, C_4H_4 and i-C_4H_5 have been performed to achieve an increase in the production rates of H_2CCCCH and C_6H_2 and a decrease of C_4H_2 production. This was obtained through balancing of the C_2H and C_4H_2 production/consumption in reactions (R2a), (R4), (R25a,b), (R30), (R31), (R32) and (R33).
It was determined that at higher temperatures, another reaction mechanism not connected to C_4H_2 production affects polyyne formation. This could be the dehydrogenation of the linear C_6H_6, which will be included in the model after an upgrade of the C_3-C_4 sub-models.

For lower temperatures (< 1300 K), formation of the first aromatics, phenyl (C_6H_5, A1-) and benzyl (C_7H_7), proceeds from precursors H_2CCCCH, i-C_4H_5 and C_5H_5. The production of the initial single-ring aromatic molecules at high temperatures (> 1300 K) is determined by the H_2CCCH recombination over the entire reaction time. Also in this case, the possible influence of the H_2CC radical on the PAH precursors was tested and any impact on the modelling results was determined. H_2CC and HOCO were discarded from the final model.
The performed study clearly determined that acetylene combustion proceeds through the strongly coupled reaction paths of fuel oxidation and PAH precursor formation; the same species are involved in these parallel processes. Therefore, the self-consistent reaction model for acetylene combustion could be obtained only by an optimisation performed on the experimental dataset encompassing both processes.

Acknowledgment

The authors wish to thank Dr.Guillaume Dayma from Institut de Combustion Aérothermique Réactivité et Environnement (ICARE), CNRS Orleans Campus for his invaluable assistance at the low-temperature ignition improvement and helpful insights in interpretation of his experimental data.

References

[1] N. Slavinskaya and P. Frank, A modelling study of aromatic soot precursor formation in laminar methane and ethene flames, Combust. Flame 156 (2009) 1705-1722.

[2] N. Slavinskaya, U. Riedel, S. Dworkin and M. Thomson, Detailed Numerical Modelling of PAH Formation and Growth in Non-Premixed Ethylene and Ethane Flames, Combust. Flame 159 (57) (2011) 979-995.

[3] V. Chernov, M. Thomson, N. Slavinskaya and U. Riedel, Soot formation with C1 and C2 fuels using an improved chemical mechanism for PAH growth, Combust. Flame 161 (2014) 592-601.

[4] M. Frenklach, Transforming data into knowledge — Process Informatics for combustion chemistry, Proc. Comb. Inst. 108 (2006) 125-140.

[5] M. Frenklach, PrIMe, [Online]. Available: https://prime-chemistry.de/. Under development.

[6] N. Slavinskaya, M. Abbasi, J. Starcke, R. Whitside, A. Mirzayeva, U. Riedel, W. Li, J. Oreluk, A. Hegde, A. Packard, M. Frenklach, G. Gerasimov and O. Shatalov, Development of an Uncertainty Quantification Predictive Chemical Reaction Model for Syngas Combustion, Energy and Fuel 31 (3) (2017) 2274-2297.

[7] R. Kee, F. Rupley and J. Miller, Chemkin-II: a FORTRAN chemical kinetics package for the analysis of gas phase chemical kinetics, Report No. SAND89-8009B, Sandia Laboratories,

1993.

[8] https://teamsites-extranet.dlr.de/vt/DLR-Mechanism/DLRMechanisms/Forms/AllItems.aspx, 2019. [Online]. Last accessed 1.08.2019.

[9] M. Frenklach, A. Packard, P. Seiler and R. Feeley, Collaborative Data Processing in Developing Predictive Models of Complex Reaction Systems, Int. J. Chem. Kinet. 36 (1) (2004) 57-66.

[10] I. Zsély, J. Zador and T. Turányi, Uncertainty analysis of NO production during methane combustion, Int. J. Chem. Kinet. 40 (2008) 754-768.

[11] T. Varga, T. Nagy, C. Olm, I. Zsély, R. Pálvölgyi, É. Valkó, G. Vincze, M. Cserháti, H. Curran and T. Turányi, Optimization of a hydrogen combustion mechanism using both direct and indirect measurements, Proc. Combus. Inst. 35 (2015) 589-596.

[12] H. Wang and D. Sheen, Combustion kinetic model uncertainty quantification, propagation and minimization, Prog. Energ. Combust. Sci. 47 (2015) 1-31.

[13] V. Kurbatov and I. Silin, New method for minimizing regular functions with constraints on parameter region, Nuclear Instruments and Methods in Physics Reserach A 345 (1994) 346-350.

[14] S. Sokolov and I. Silin, Preprint JINR D-810, Dubna, 1961.

[15] L. Fokin and N. Slavinskaya, Thermo-physical parameter correlation for low-density gas-mixtures – Ar–Xe, Institute for High Temperatures, Institute for High Temperatures, USSR Academy of Sciences 25 (1) (1987) 40-45.

[16] K. Hughes, T. Turanyi, A. Clague and M. Pilling, Development and testing of a comprehensive chemical mechanism for the oxidation of methane, Int. J. Chem. Kinet. 33 (2001) 513-538.

[17] J. Warnatz, H. Bockhorn, A. Moser and H. Wenz, Experimental investigations and computational simulation of acetylene-oxygen flames from near stoichiometric to sooting conditions, Proc. Combust. Inst. 19 (1982) 197-209.

[18] Y. Tan, P. Dagut, M. Cathonnet and J. Boettner, Acetylene oxidation in a JSR from 1 to 10atm and comprehensive kinetic modeling, Combust. Sci. Technol. 102 (1994) 21-55.

[19] J. Miller, J. Volponi and J. Pauwels, The effect of allene addition on the structure of a rich $C_2H_2/O_2/Ar$ flame, Combust. Flame 105 (1996) 451-461.

[20] Y. Hidaka, K. Hattori, T. Okuno, K. Inami, T. Abe and T. Koike, Shock-tube and modeling study of acetylene pyrolysis and oxidation, Combust. Flame 107 (1996) 401-417.

[21] R. Lindstedt and G. Skevis, Chemistry of Acetylene Flames, Combust. Sci. Technol. 125 (1997) 73-137.

[22] B. Varatharajan and F. Williams, Chemical-kinetic descriptions of high-temperature ignition and detonation of acetylene-oxygen-diluent systems, Combust. Flame 125 (2001) 624-645.

[23] N. Leplat, P. Dagaut, C. Togb and J. Vandooren, Numerical and experimental study of ethanol combustion and oxidation in laminar premixed flames and in jet-stirred reactor, Combust.

Flame 158 (2011) 705-725.

[24] W. Metcalfe, S. Burke, S. Ahmed and H. Curran, A Hierarchical and Comparative Kinetic Modeling Study of $C_1 - C_2$ Hydrocarbon and Oxygenated Fuels, J. Chem. Kinet. 45 (2013) 638-675.

[25] K. Leung and R. Lindstedt, Detailed kinetic modeling of C1—C3 alkane diffusion flames, Combust. Flame 102 (1995) 129-160.

[26] B. Eiteneer and M. Frenklach, Experimental and modeling study of shock-tube oxidation of acetylene, Int. J. Chem. Kinet. 35 (2003) 391–414.

[27] J. Gimenez-Lopez, C. Rasmussen, H. Hashemi, M. Alzueta, Y. Gao, P. Marshall, C. Goldsmith, P.Glaborg, Experimental and kinetic modeling study of C_2H_2 oxidation, Int. J. Chem. Kinet. 48 (11) (2016) 724–738.

[28] B.-Y. Wang, Y.-X. Liu, J.-J. Weng, P. Glaborg and Z.-Y. Tian, New insights in the low-temperature oxidation of acetylene, Proc. Comb. Inst. 36 (2017) 355-363.

[29] C. Goldsmith, L. Harding, Y. Georgievskii, J. Miller and S. Klippenstein, Temperature and Pressure-Dependent Rate Coefficients for the Reaction of Vinyl Radical with Molecular Oxygen, J. Phys. Chem. A 119 (2015) 7766-7779.

[30] A. Laskin and H. Wang, On initiation reactions of acetylene oxidation in shock tubes: A quantum mechanical and kinetic modeling study, Chem. Phys. Lett. 303 (1999) 43-49.

[31] M. Alzueta, M. Borruey, A. Callejas, A. Millera and R. Bilbao, An experimental and modeling study of the oxidation of acetylene in a flow reactor, Combust. Flame 152 (2008) 377–386.

[32] J. Miller and C. Melius, Kinetic and thermodynamic issues in the formation of aromatic compounds in flames of aliphatic fuels, Combust. Flame 91 (1992) 21-39.

[33] W. Tsang and R. Hampson, Chemical Kinetic Data Base for Combustion Chemistry. Part I. Methane and Related Compounds, J. Phys. Chem. Ref. Data 15 (1986) 1087-1279.

[34] J. Senosiain, S. Klippenstein and J. Miller, The Reaction of Acetylene with Hydroxyl Radicals, J. Phys. Chem. A 109 (2005) 6045.

[35] A. Liu, W. Mulac and C. Jonah, Temperature dependence of the rate constants of the reactions of hydroxyl radicals with acetylene and acetylene-d2 at 1 atm in argon from 333 to 1273 K, J. Phys. Chem. 92 (1988) 5942-5945.

[36] J. Vandooren and P. Van Tiggelen, Reaction mechanisms of combustion in low pressure acetylene-oxygen flames, Symp. Combust. Proc. 16 (1976) 1133-1144.

[37] I. Woods und B. Haynes, C1/C2 chemistry in fuel-rich post-flame gases: Detailed kinetic modelling, Symp. (Int.) Combust. 25 (1994) 909-917.

[38] J. Miller and C. Melius, A theoretical analysis of the reaction between hydroxyl and acetylene, Proc. Combust. Inst. 22 (1989) 1031-1039.

[39] D. Baulch, C. Cobos, R. Cox, P. Frank, G. Hayman and et al., Evaluated Kinetic Data for Combustion Modeling. Supplement I, J. Phys. Chem. Ref. Data 23 (1994) 847-1031.

[40] J. Michael and A. Wagner, Rate constants for the reactions O + C_2H_2 and O + C_2D_2 → products, over the temperature range ≈ 850-1950 K, by the flash photolysis-shock tube technique. Determination of the branching ratio and a further theoretical analysis, J. Phys. Chem. 94 (1990) 2453-2464.

[41] N. Marinov, W. Pitz, C. Westbrook, M. Castaldi and S. Senkan, Modeling of Aromatic and Polycyclic Aromatic Hydrocarbon Formation in Premixed Methane and Ethane Flames, Combust. Sci. Technol.1996 116 (1) (1996) 211-287.

[42] P. Frank, K. Bhaskaran and T. Just, Acetylene oxidation: The reaction C_2H_2+O at high temperatures, Proc. Combust. Inst. 21 (1988) 885-893.

[43] D. Baulch, C. Bowman, C. Cobos and et al., Evaluated Kinetic Data for Combustion Modeling: Supplement II, J. Phys. Chem. Ref. Data 34 (3) (2005) 757.

[44] J. Warnatz, Rate coefficients in the C/H/O system, in Combustion Chemistry, NY, Springer-Verlag, 1984.

[45] T. Nguyen, L. Vereecken and J. Peeters, Quantum Chemical and Theoretical Kinetics Study of the O(^{3}P) + C_2H_2 Reaction: A Multistate Process, J. Phys. Chem. A 110 (2006) 66920.

[46] R. Lohr and P. Roth, Shock tube measurements of the reaction behaviour of acetylene with O-atoms, Ber. Bunsenges. Phys. Chem. 85 (1981) 153-158.

[47] G. Smith, D. Golden, M. Frenklach and et al., GRI-Mech 3.0, [Online]. Available: http://combustion.berkeley.edu/gri-mech/version30/text30.html Last accessed: 31.07.2019.

[48] A. Konnov, Implementation of the NCN pathway of prompt-NO formation in the detailed reaction mechanism, Combust. Flame 156 (2009) 2093-2105.

[49] L. Harding, Y. Georgievskii and S. Klippenstein, Predictive Theory for Hydrogen Atom−Hydrocarbon Radical Association Kinetics, J. Phys. Chem A 109 (2005) 4646-4656.

[50] J. Miller and S. Klippenstein, The H + C_2H_2 (+M) ⇄ C_2H_3 (+M) and H + C_2H_2 (+M) ⇄ C_2H_5 (+M) reactions: Electronic structure, variational transition-state theory, and solutions to a two-dimensional master equation, Phys. Chem. Chem. Phys. 6 (2004) 1192-1202.

[51] V. Knyazev and I. Slagle, Experimental and Theoretical Study of the C_2H_3 ⇄ H + C_2H_2 Reaction. Tunneling and the Shape of Falloff Curves, J. Phys. Chem. 100 (1996) 16899-16911.

[52] J. Michael, M.-C. Su, J. Sutherland, L. Harding and A. Wagner, Rate Constants for D + C_2H_2 → C_2HD + H at High Temperature: Implications to the High Pressure Rate Constant for H + C_2H_2 → C_2H_3, J. Phys. Chem. A 107 (2003) 10533-10543.

[53] M. Rickard, J. Hall and E. Petersen, Effect of silane addition on acetylene ignition behind reflected shock waves, Proceedings of the Combustion Institute 30 (2 (2005) 1915-1923.

[54] Y. Hidaka, C. Eubank, J. Gardiner and S. Hwang, Shock Tube and Modeling Study of Acetylene Oxidation, J. Phys. Chem. 88 (1984) 1006-1012.

[55] R. Fournet, J. Bauge and F. Battin-Leclerc, Experimental and Modeling of Oxidation of Acetylene, Propyne, Allene and 1,3-Butadiene, Inc. Int. J. Chem. Kinet. 31 (1999) 361-379.

[56] F. Egolfopoulous, D. Zhu and C. Law, Experimental and Numerical Determination of Laminar Flame Speeds: Mixtures of C,·Hydrocarbons with Oxygen and Nitrogen, Proc. Combust. Inst. 23 (1991) 471-478.

[57] G. Jomaas, X. Zheng, D. Zhu and C. Law, Experimental determination of counterflow ignition temperatures and laminar flame speeds of C2–C3 hydrocarbons at atmospheric and elevated pressures, Proc. Combust. Inst. 30 (2005) 193-200.

[58] O. Park, P. Veloo and E. F. N., Flame studies of C2 hydrocarbons, Proc. Combust. Inst. 34 (2013) 711-718.

[59] S. Ravi, T. Sikes, A. Morones, C. Keesee and E. Petersen, Comparative study on the laminar flame speed enhancement of methane with ethane and ethylene addition, Proc. Combust. Inst. 35 (1) (2015) 679–686.

[60] X. Shen, X. Yang, J. Santer, J. Sun and Y. Ju, Experimental and kinetic studies of acetylene flames at elevated pressures, Proc. Combust. Inst. 35 (2015) 721-728.

[61] E. Rokni, A. Moghaddas, O. Askari and H. Metghalchi, Measurement of Laminar Burning Speeds and Investigation of Flame Stability of Acetylene (C2H2)/Air Mixtures, Journal of Energy Resources Technology 137 (1) (2014) 012204.

[62] Kintech Lab Ltd. Chemical Workbench®, [Online]. Available: http://www.kintechlab.com/. Last accessed: 31.07.2019.

[63] S. Klippenstein, J. Miller and L. Harding, Resolving the mystery of prompt CO_2: The $HCCO+O_2$ reaction, Proc. Combust. Inst. 29 (2002) 1209-1217.

[64] A. Mebel, E. Diau, M. Lin and K. Morokuma, Ab initio and RRKM calculations for multichannel rate constants of the C2H3 + O2 reaction, J. Am. Chem. Soc.,vol. 188 (1996) 9759-9771.

[65] H. Hashemi, J. Jacobsen, C. Rasmussen, J. Christensen, P. Glarborg, S. Gersen, M. Essen, H. Levinsky and S. Klippenstein, High-pressure oxidation of ethane, Combust. Flame 182 (2017) 150–166.

[66] G. Da Silva and J. Bozzelli, Variational Analysis of the Phenyl + O2 and Phenoxy + O Reactions, J. Phys. Chem. A 112 (2008) 3566-3575.

[67] M. B. Colket, The pyrolysis of acetylene and vinylacetylene in a single-pulse shock tube, Proc. Combust. Inst. 21 (1) (1988) 851-864.

[68] C. H. Wu, H. J. Singh and R. D. Kern, Pyrolysis of Acetylene Behind Reflected Shock Waves, Int. J. Chem. Kinet. 19 (1987) 975-996.

[69] R. D. Kern, K. Xie, H. Chen and J. H. Kiefer, High temperature pyrolyses of avetylene and diacetylene behind reflected shock waves, Proc. Combust. Inst. 23 (1990) 69-75.

[70] M. Aghsaee, S. Dürrstein, J. Herzler, H. Böhm, M. Fikri and C. Schulz, Influence of molecular hydrogen on acetylene pyrolysis: Experiment and modeling, Combust. Flame 161 (2014) 2263–2269.

[71] P. R. Westmoreland, J. B. Howard und J. P. Longwell, Tests of published mechanisms by

comparison with measured laminar flame structure in fuel-rich acetylene combustion, Symp. (Int.) Combust. 21 (1988) 773-800.

[72] E. Bastin, D. J.-L., M. Reuillon, V. C. and J. Warnatz, Experimental and computational investigation of the structure of a sooting C2H2-O2-Ar flame, Symp. (Int.) Combust. 22 (1988) 313-322.

[73] A. Lamprecht, B. Atakan and K. Kohse-Höinghaus, Fuel-rich Propene and Acetylene Flames: A Comparison of Their Flame Chemistries, Combust.Flame 122 (2000) 483–491.

[74] K. Norinaga, V. M. Janardhanan and O. Deutschmann, Detailed chemical kinetic modeling of pyrolysis of ethylene, acetylene, and propylene at 1073–1373 K with a plug-flow reactor model, Int J Chem Kinet 40 (4) (2008) 199-208.

[75] N. E. Sanchez, A. Millera, R. Bilbao and M. U. Alzueta, Polycyclic aromatic hydrocarbons (PAH), soot and light gases formed in thepyrolysis of acetylene at different temperatures: Effect of fuel concentration, J. Analyt. and Appl. Pyrol. 103 (2013) 126–133.

[76] S. Klippenstein and J. Miller, The addition of hydrogen atoms to diacetylene and the heats of formation of i-C4H3 and n-C4H3, J. Phys. Chem. A 109 (2005) 4285-4295.

[77] I. Slagle, J. Bernhardt and D. Gutman, Kinetics of the reactions of unsaturated free radicals (methylvinyl and i-C4H3) with molecular oxygen, Symp. Int. Combust. Proc. 22 (1989) 953-962.

[78] T. Tanzawa and W. C. J. Gardiner, Thermal decomposition of acetylene, Symp. Int. Combust. Proc. 17 (1978) 563-572.

[79] A. Dean, Predictions of pressure and temperature effects upon radical addition and recombination reactions, J. Phys. Chem. 89 (1985) 4600-4608.

[80] M. Weissman and S. Benson, Rate parameters for the reactions of C2H3 and C4H5 with H2 and C2H2, J. Phys. Chem. 92 (1988) 4080-4084.

[81] C. Saggese, N. E. Sánchez, A. Frassoldati, A. Cuoci, T. Faravelli, M. U. Alzueta and E. Ranzi, A Kinetic Modeling Study of Polycyclic Aromatic Hydrocarbons (PAHs) and Soot Formation in Acetylene Pyrolysis, Energy Fuels 28 (2) (2014) 1489-1501.

[82] J. Zador, M. D. Fellows, J. A. Miller, Initiation Reactions in Acetylene Pyrolysis, J. Phys. Chem. A 121 (2017) 4203-4217.

[83] F. Battin-Leclerc, J. M. Simmie, E. Blurock, Cleaner combustion: developing detailed chemical kinetic models, Springer, London, 2013.

[84] H. Cutler, M. J. Antal, Jr., M. Jones, Jr., A Critical Evaluation of the Plug-Flow Idealization of Tubular-Flow Reactor Data, Ind. Eng. Chem. Res. 27 (1988) 691-697.

[85] S. V. Ramayya, M. J. Antal, Jr., Evaluation of Systematic Error Incurred in the Plug Flow Idealization of Tubular Flow Reactor Data, Energy Fuels 3 (1989) 105-108.

[86] J. B. Rawlings, J. G. Ekerdt, Chemical Reactor Analysis and Design Fundamentals, Madison, Wis. : Nob Hill Pub., 2002, 609 p.

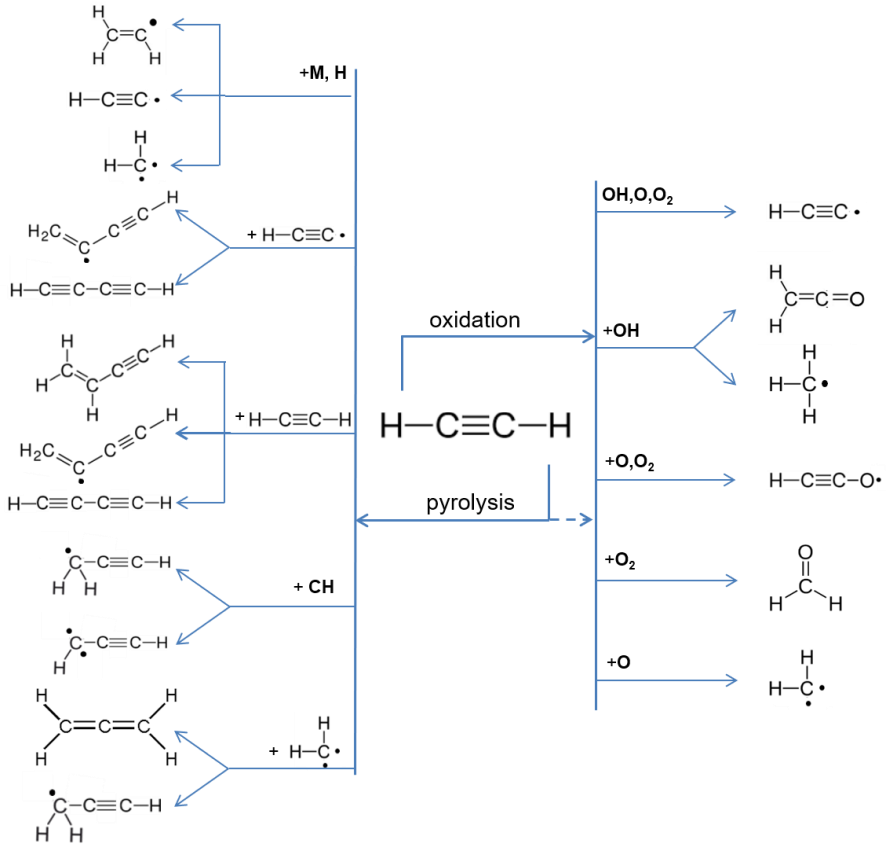

Figure 1. The major initial stages of acetylene oxidation and pyrolysis adopted in the present model.

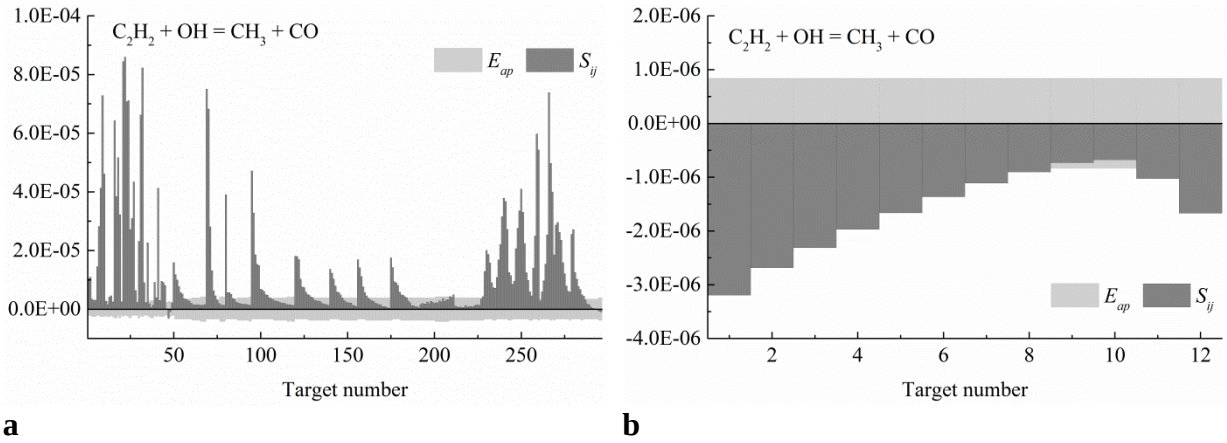

a **b**

Figure 2. Comparison of the normalised integrated sensitivity coefficients, S_{ij}, of a) ignition delay times and b) laminar flame speed to reaction rate coefficient for C_2H_2 + OH ↔ CH_3+CO with a criterion for applicability of experimental target for reaction rate improvement, E_{ap}.

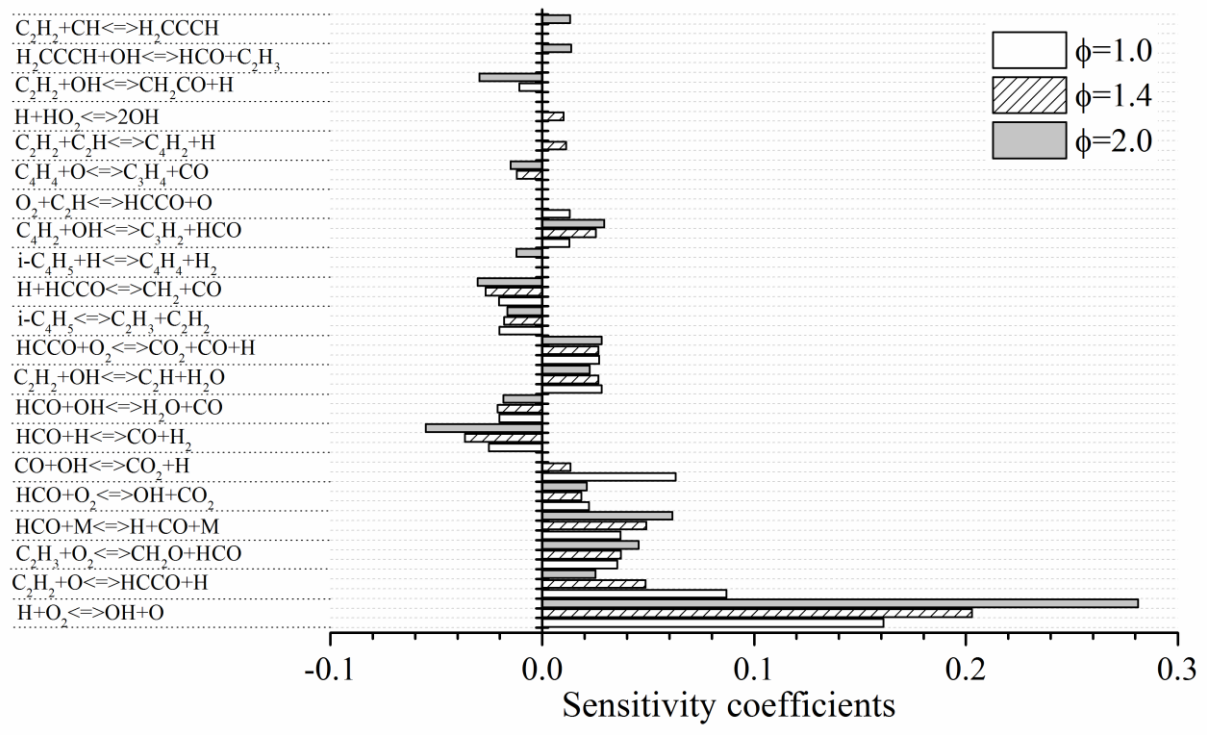

Figure 3. Logarithmic response sensitivities of the laminar flame speed computed with Model-1 for data measured at p = 1 atm, T_0 = 298 K, ϕ = 0.6, 1.4 and 2.0.

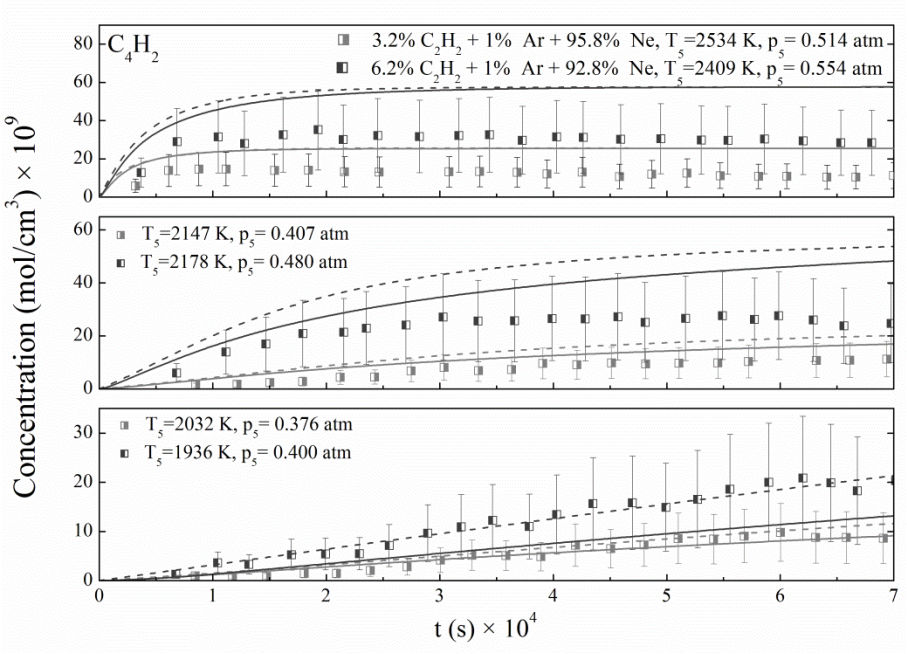

a

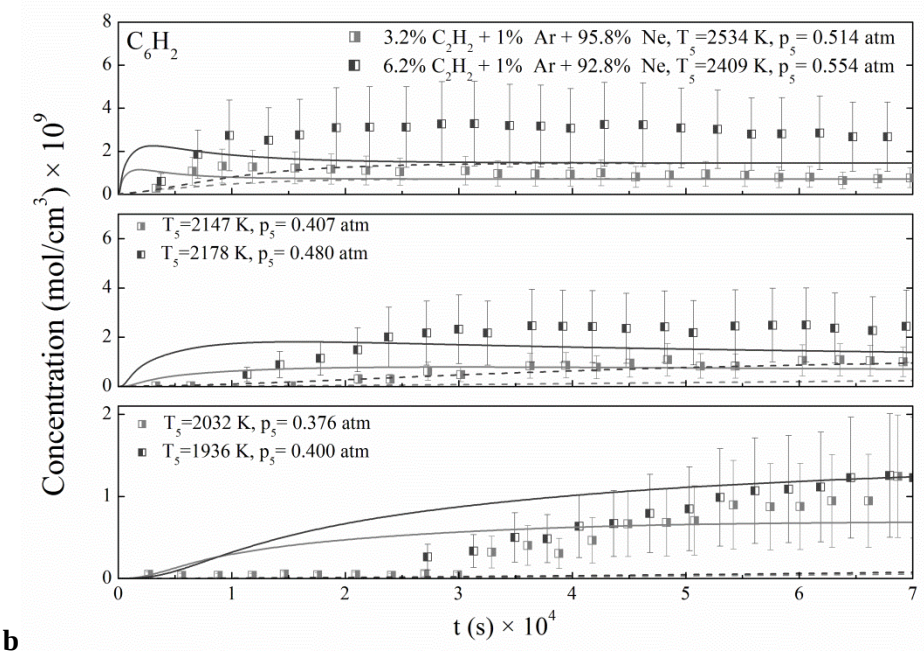

b

Figure 4. Comparison of concentration profiles measured by Wu *et al.* [68] in the shock tube pyrolysis of C_2H_2 with simulations using Model-2 (dashed lines) and the final Model (solid lines) .

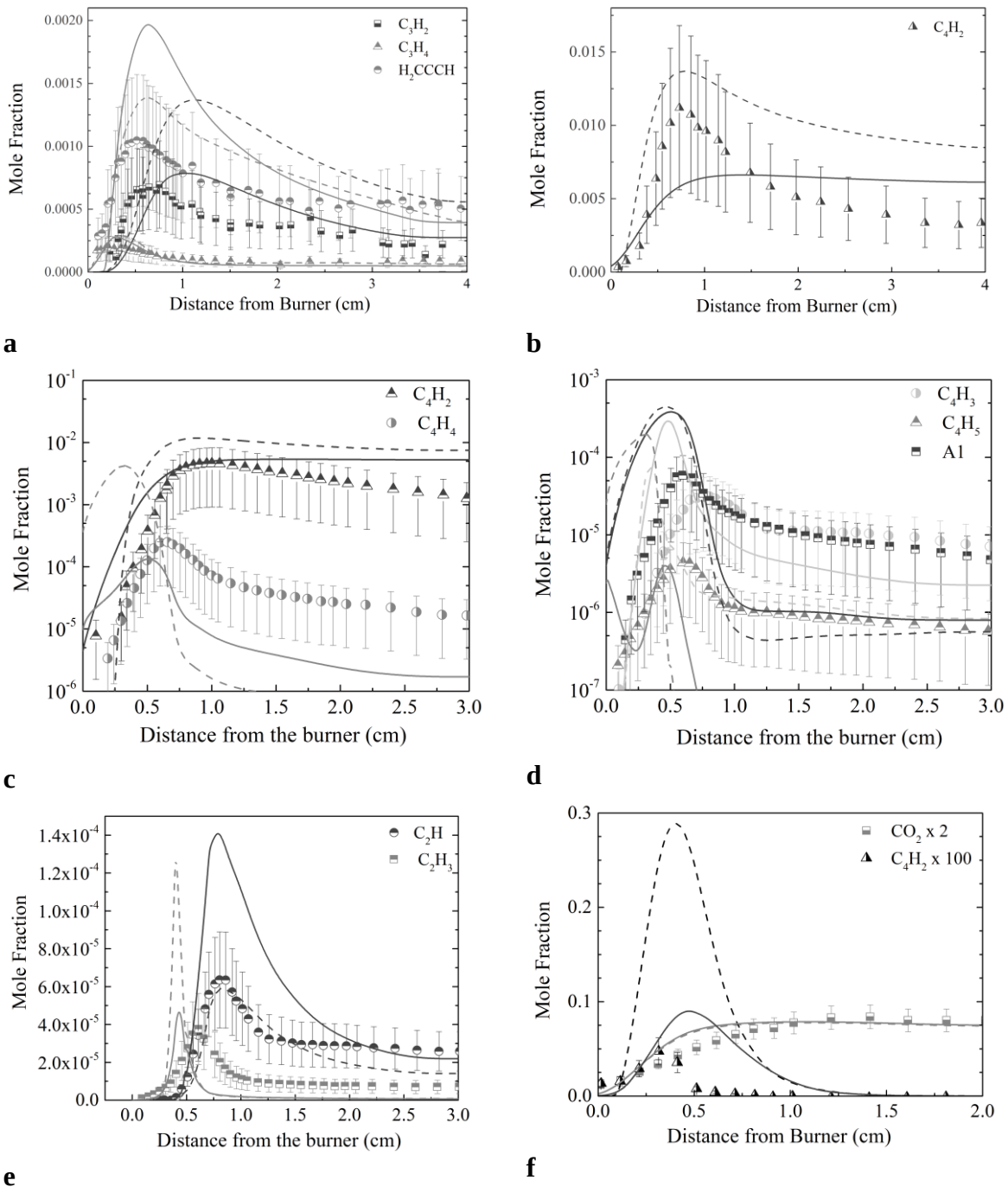

Figure 5. Comparison of concentration profiles measured in the laminar flame of C_2H_2 by a,b) Westmoreland *et al.* [71], 46.5%C_2H_2/48.5%O_2/5%Ar, p = 2.67 kPa; c,d,e) by Bastin *et al.* [72], 27.5%C_2H_2/27.5%O_2/45%Ar, p = 2.6 kPa; f) by Miller *et al.*[19], 12.96% C_2H_2 + 19.44% O_2 + 67.6% Ar, p = 25 Torr, with simulations using Model-2 (dashed lines) and the final Model (solid lines).

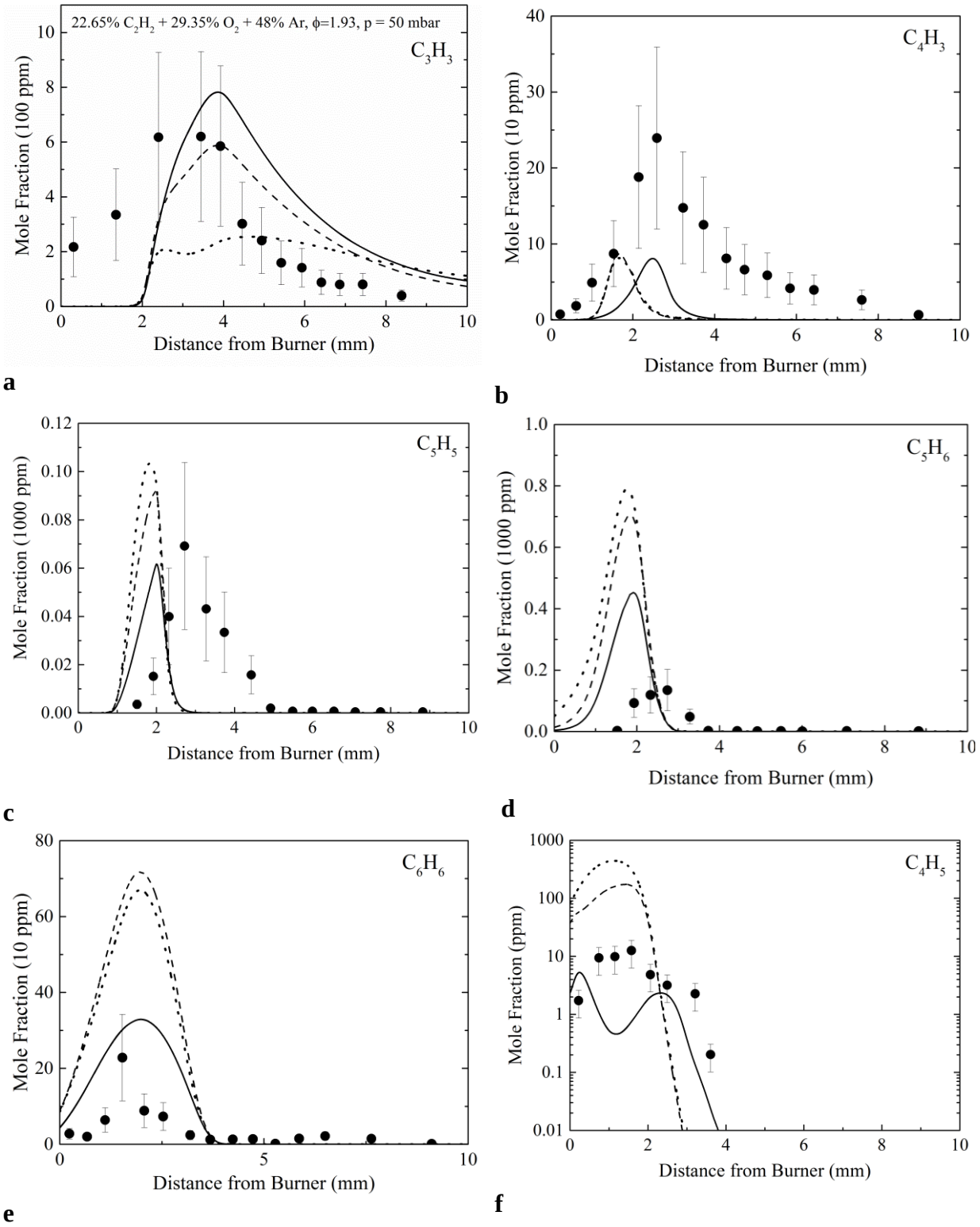

Figure 6. Comparison of concentration profiles measured by Lamprecht *et al.* [73] in a laminar flame of C_2H_2 with simulations using Model-1 (dotted lines), Model-2 (dashed lines) and the final Model (solid lines).

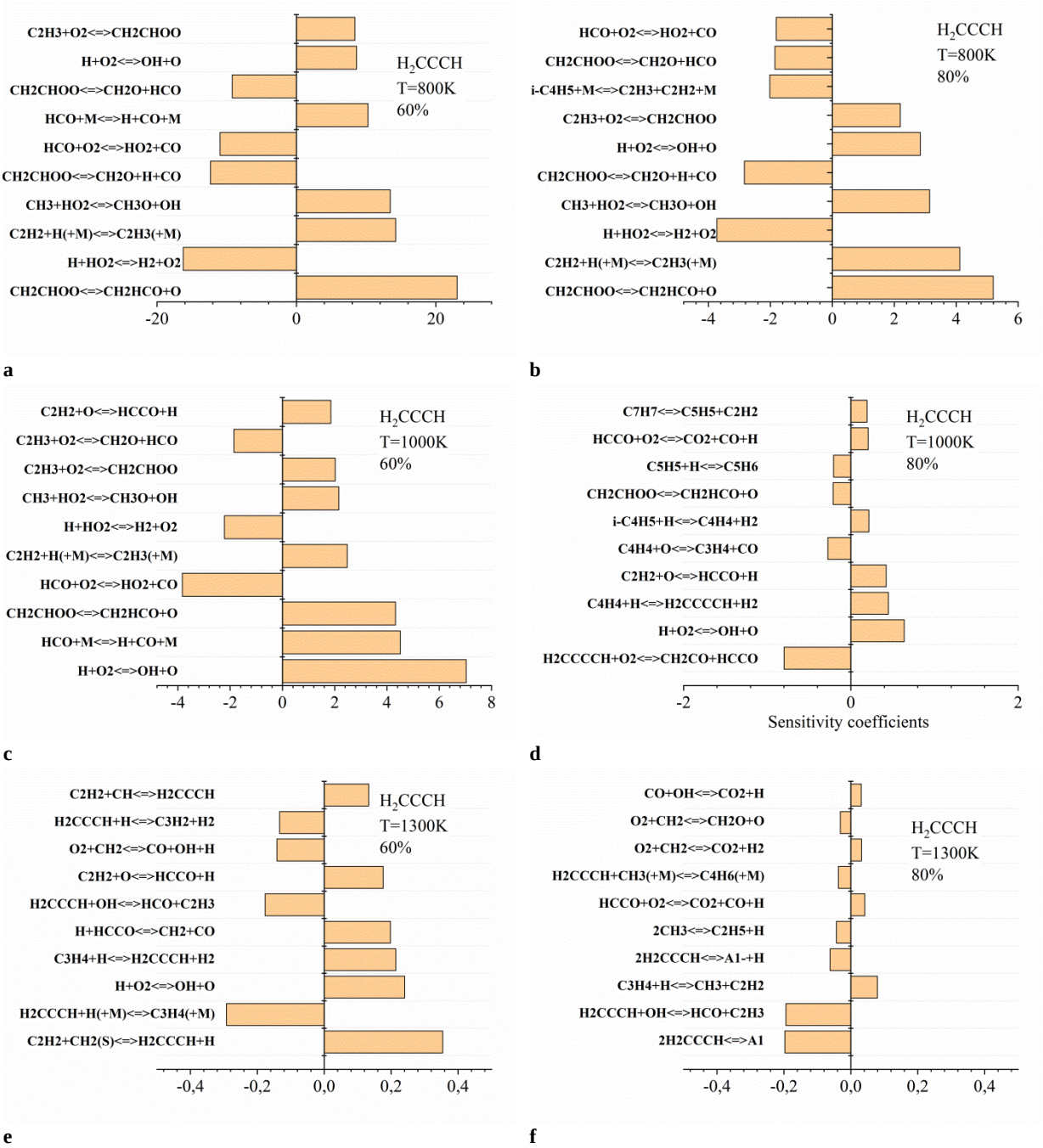

Figure 7. Sensitivity coefficients for H2CCCH calculated for mixture with ϕ=2 from [28] **with the final Model for different initial temperature (the first 10 most important reactions are shown).**

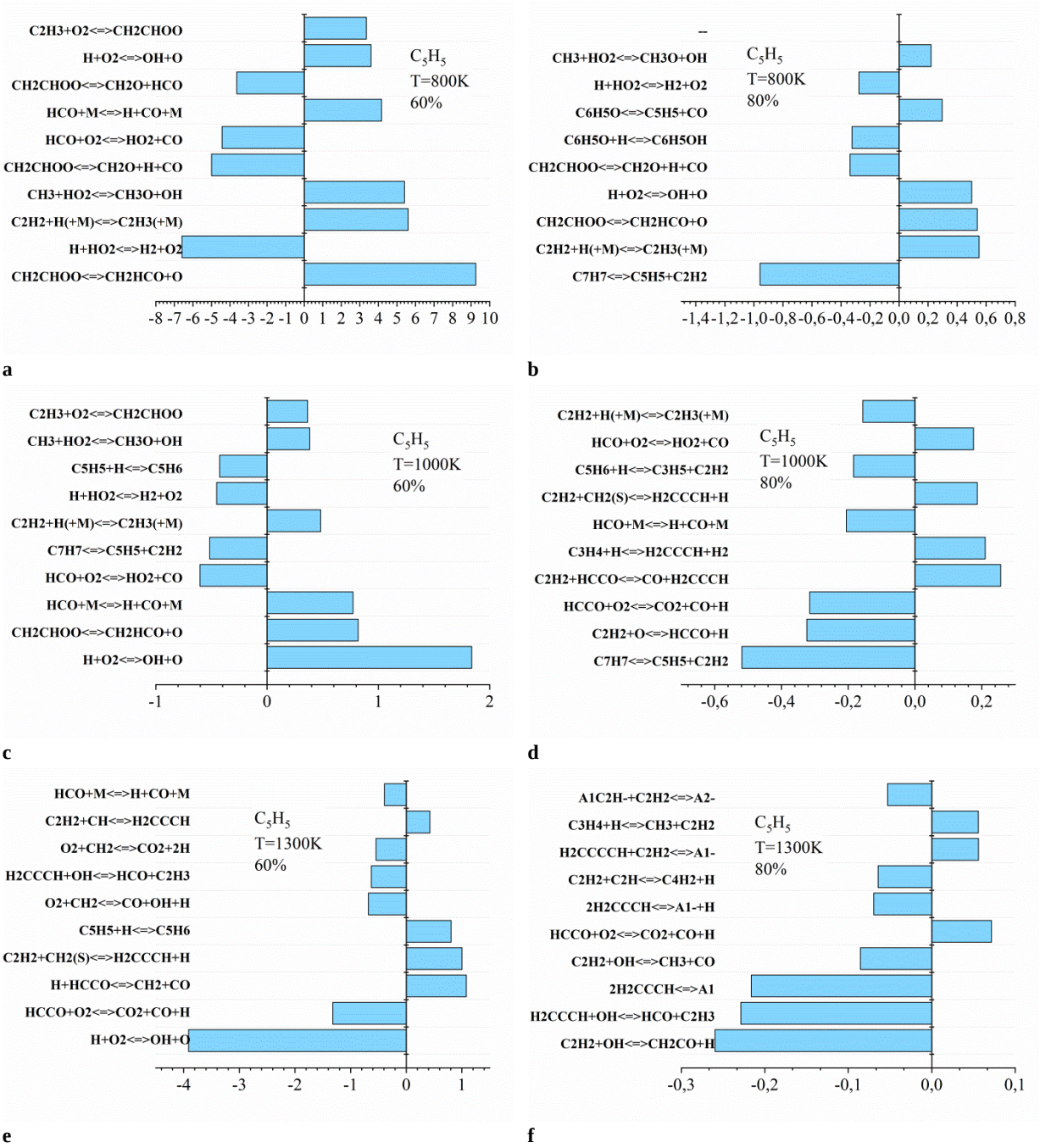

Figure 8. Sensitivity coefficients for C_5H_5 calculated for mixture with ϕ=2 from [28] **with the final Model for different initial temperature (the first 10 most important reactions are shown).**

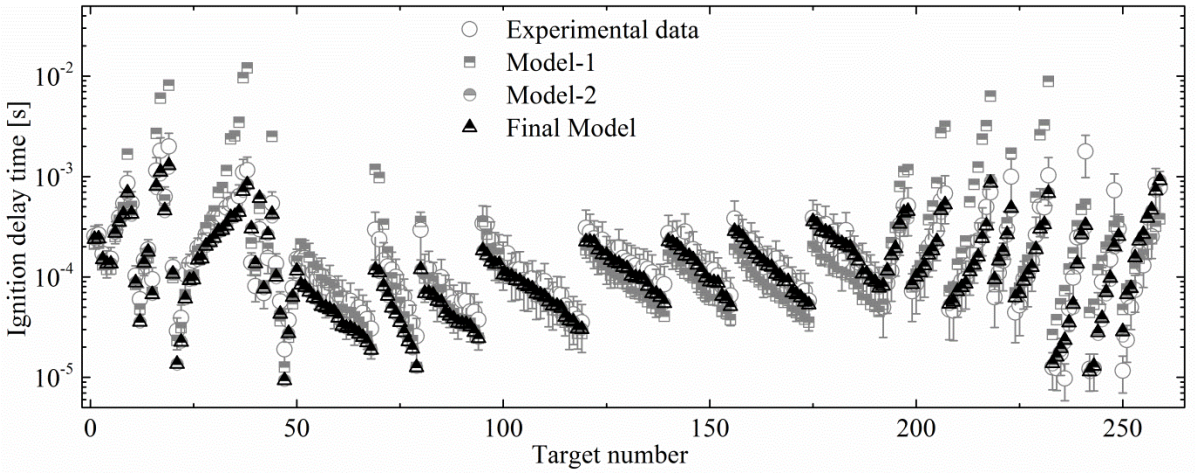

Figure 9. Comparison of experimental ignition delay data versus simulations performed with Model-1, Model-2 and the final Model (Details are in Supplement-5).

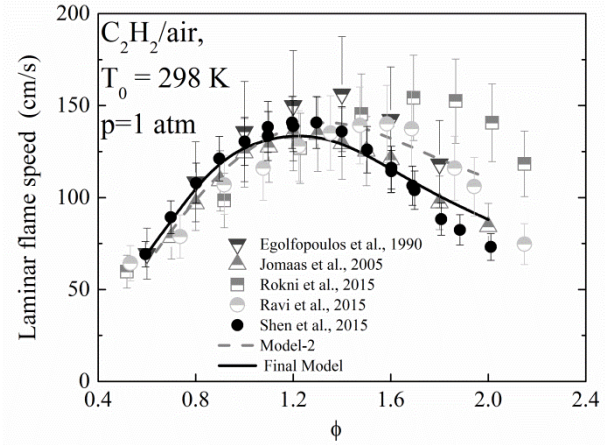

Figure 10. Experimental laminar flame speed data [56, 57, 59-61] versus simulations performed with Model-2 and the final Model.

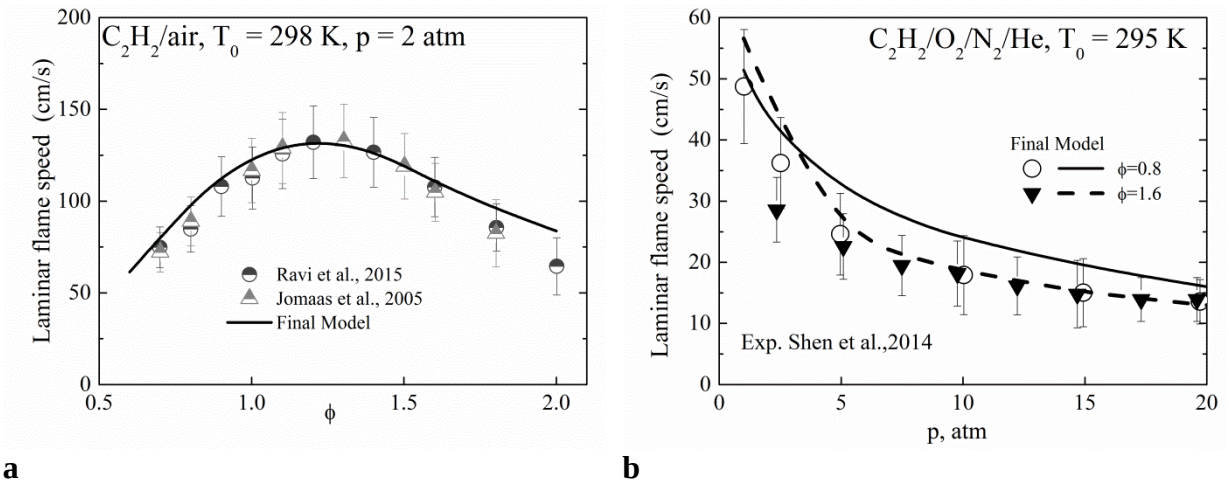

Figure 11. Experimental laminar flame speed data [57, 59, 60] versus simulations performed with the final Model.

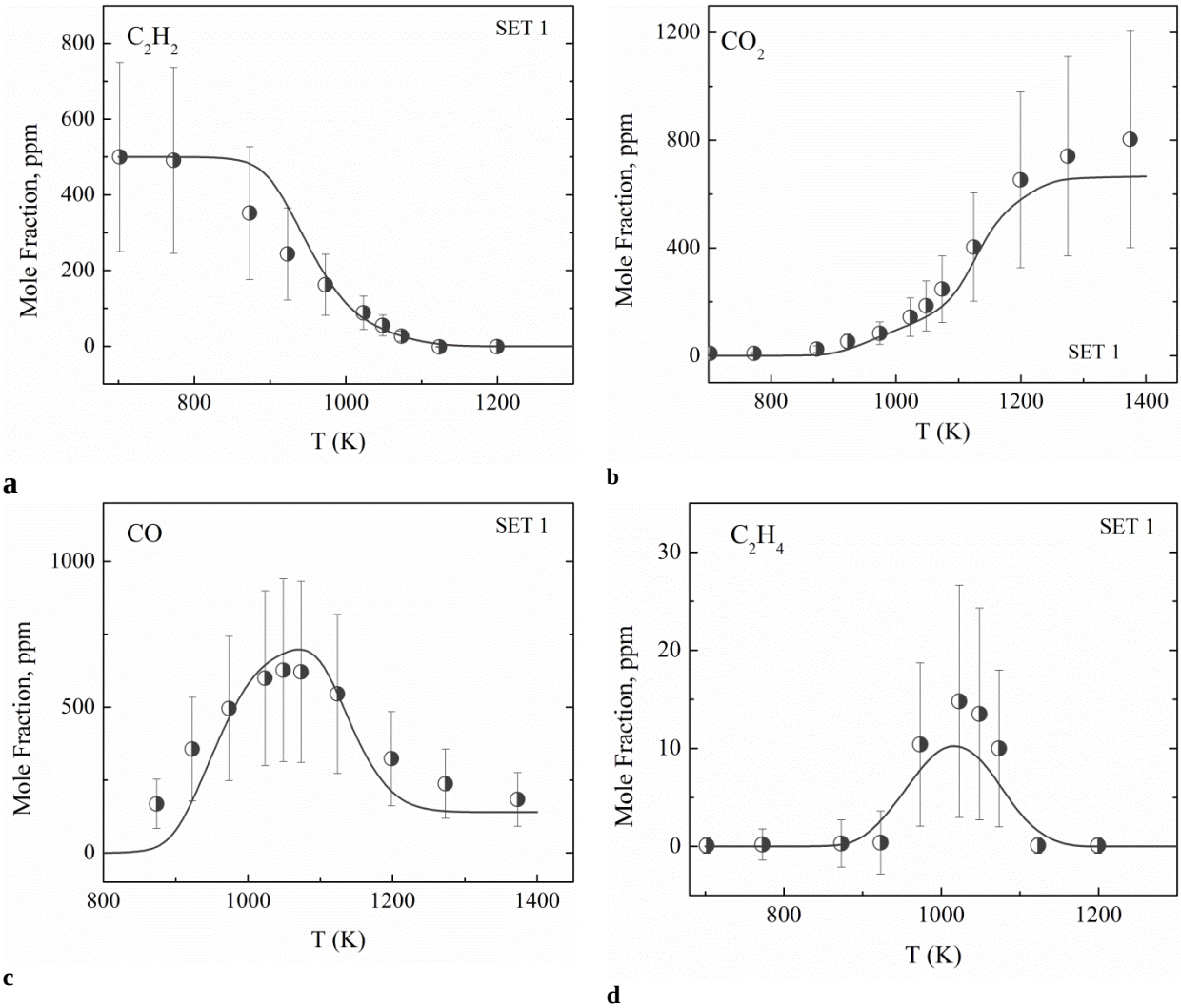

Figure 12. Comparison of concentration profiles measured by Alzueta *et al.* [31] for acetylene oxidation in a PFR, 500ppmC_2H_2/875 ppmO_2/7000ppmH_2O, p=1atm, with simulations using the final Model (lines).

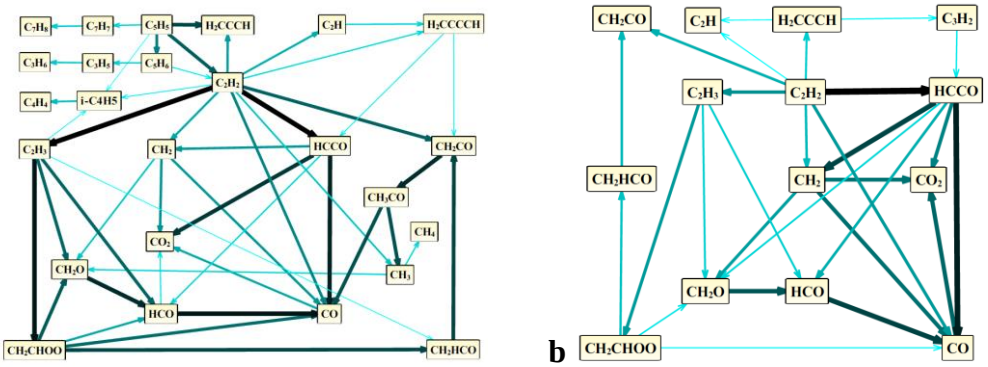

Figure 13. The reaction flow diagram of C_2H_2 oxidation for T_5 = 1150 K, p_5 = 1 atm, ϕ = 1: a) 30% and b) 80% of fuel consumption.

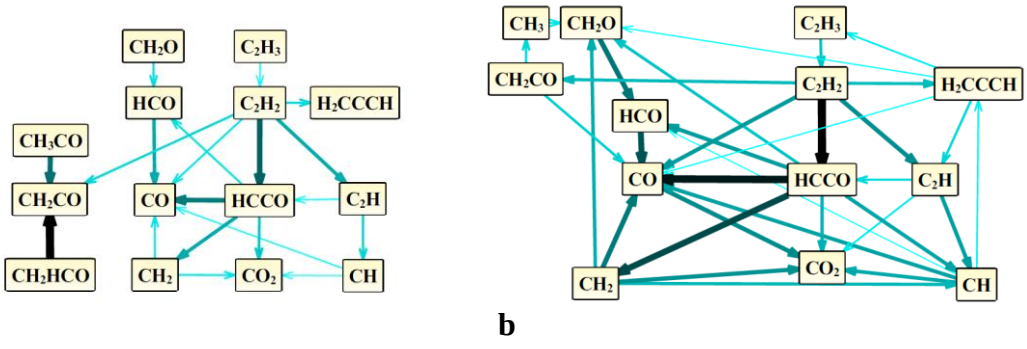

Figure 14. The reaction flow diagram of C_2H_2 oxidation for T_5 = 1650 K, p_5 = 1 atm, ϕ = 1; a) 30% and b) 80% of fuel consumption.